Dear **Referee #1**,

Thank you for your insightful comments on the manuscript and for providing advice on how to improve it. We appreciate your time. The manuscript has been considerably reworked following your comments and those of Referee #2.

The title and objectives have been reworded to reflect our focus on the combined use of TerraSAR-X and time-lapse photography for seasonal sea ice processes monitoring. Section 2“SAR backscattering from sea ice” has been removed. The methods and results have been re-organized and some content has been moved to the supplementary materials. The discussion has been completely rewritten.

We reproduced your comments below (R), provided our answers (A), and detailed changes to the manuscript (M). When providing section numbers, we refer to the first version of the manuscript.

SDB

Anonymous Referee #1

R1: My major concern with this paper now is how authors have justified the similarity in the backscatter evolution of X-band and C-band. See Line 485 under section 7.2. "The TerraSAR-X backscattering time-series presented in this article exhibits the same seasonal evolution as that of the C-band (Sect. 2), which was expected due to the spectral proximity of both bands." This sentence reads like the author already knew about the results and as an afterthought. This has lead to authors more or less assuming the scattering mechanisms during the seasonal evolution (like that with C-band), based on past literature. This is scientifically misleading. If there was similarity in scattering mechanisms at two different frequencies, our scientific community wouldn’t have launched TerraSAR-X and RADARSAT-2 (for e.g.).
A1: All assumptions of similarity between both bands have been removed from the manuscript. Comparison of the X-band data with the literature on C-band is now reserved for the discussion.
M1:
Section “2. SAR backscattering over snow-covered sea ice”, which presented a literature review on the seasonal evolution of C-band backscattering from first-year sea ice, was removed following your comments as well as those of Referee #2. Relevant references to the literature on this topic are now reserved for the discussion.
In the Methods, the seasonal features consistently observed throughout the acquisition parameters and years of the study are no longer associated to physical processes or mechanisms:

> *“Recurring seasonal features in all X-band VV median backscattering time-series acquired during this study include two peaks separated by a monotone period. From this, four indicators were derived: the post-freeze-up peak (I), the beginning (II) and*

end (III) of the monotone period, and the spring peak (IV). Examples are shown in Fig. 4 for two different years and orbits, chosen for their clarity.

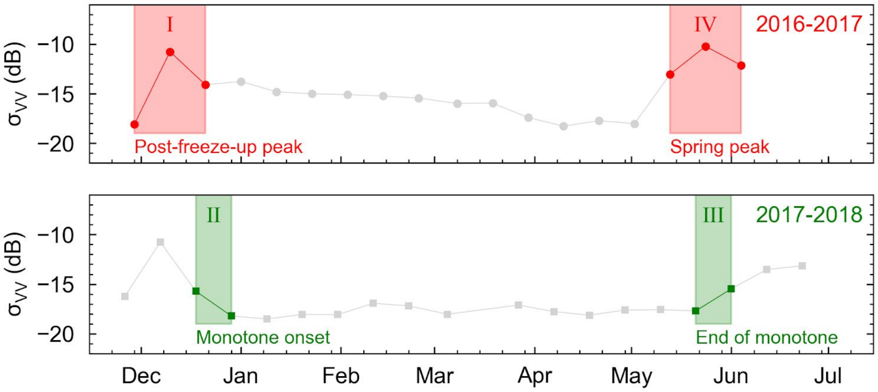

> ***Figure 4**: Examples of change detection in TerraSAR-X VV median backscattering. Peak detection for orbit 21 in 2016-2017 (top), and inflexion detection for orbit 13 in 2017-2018 (bottom).”*
> *(in the Methods)*

In the Discussion, each seasonal feature is examined in terms of potential scattering mechanisms.

> *“The post-freeze-up peak and monotone backscattering onset are also observed in C-band time-series over sea ice (Yackel et al., 2007), but these features have been less studied than their spring counterparts (end of monotone backscattering and spring peak). Moreover, the same features in the X and C-band could well be related to different scattering mechanisms, and even to different physical processes. We limit ourselves to speculating, for the X-band data presented in this manuscript, that the increasing portion of the peak may be associated with the domination of surface scattering related to a brine-rich ice surface, potentially covered in frost flower, and that the decreasing portion may be associated with a transition to a dispersion regime, in which the signal suffers loss in the brine-wetted and increasingly colder snow. ” (in the Discussion)*

R2: a) Although the objective of this manuscript was to focus more on how X-band SAR can be used to provide the first-baseline signature of X-band VV backscatter. However, the majority of the paper is about analyses from time-lapse photographs and very little focus was given to analyzing the SAR signature section. I would suggest using the SAR images as the focal point of analysis (with snow/sea-ice geophysical explanation of changes in VV backscatter), ’supported’ by time-lapse photography.

A2: The manuscript title and objectives were reworded to clarify the focus of the work, which is on the combined use of TerraSAR-X and time-lapse photography time-series for the seasonal monitoring of sea ice processes. Both observational tools are uniquely qualified for remote applications, for instance in polar regions, and are often used as stand-alone tools. However, they provide access to different aspects of the environment they observe, and have different strengths (e.g. photography allows for hourly acquisitions, but with a limited view, while SAR remote sensing has a wide and precise spatial coverage, but with fewer acquisitions). We chose to give equal importance to the two data sources to explore their complementarity. The manuscript has been reworked to focus on this objective. The Methods and Discussion sections have been reorganized in the following way: first, each data source is treated as a stand-alone monitoring tool, and second, the two data sources are co-interpreted.

M2:

Reworded Title:

> *“Combining TerraSAR-X and time-lapse photography for seasonal sea ice monitoring: the case of Deception Bay, Nunavik” (Title)*

Reworded manuscript objectives:

> *“This article explores the use of combined TerraSAR-X and time-lapse photography time-series to observe seasonal sea ice processes, and the potential of the time-lapse photography to support TerraSAR-X interpretation. The case study is performed over three years in Nunavik’s Deception Bay. A complementary objective is to describe the processes through an interannual comparison. (in the Introduction)*

The Methods have been expanded and reorganized to clarify our parallel use of photograph interpretation and TerraSAR-X image interpretation, and their co-interpretation:

> *“[...] Sections 4.1 and 4.2 describe the indicators and how they are observed or measured from each data source. Section 4.3 then explains how photographs are compared with coincident satellite images and used to identify their features, which serves to evaluate the potential of time-lapse photography to enhance TerraSAR-X image interpretation.” (in the Methods)*

The Discussion has been rewritten:

> *“The use of TerraSAR-X and time-lapse photography time-series for seasonal monitoring of sea ice processes is first discussed for each data source as a stand-alone monitoring tool (Sect. 6.1), and then for their combination (Sect. 6.2). This discussion focuses on three aspects of sea ice processes which are accessible with these tools: temporal, spatial, and spectral. Section 6.3 then discusses seasonal sea ice processes observed using combined TerraSAR-X and time-lapse photography time-series.” (in the Discussion)*

R3: b) how they classified ice types (what method) from the TerraSAR-X images, based on beta-naught values? What is the advantage of using beta-naught over traditional sigma-naught? The authors may be reminded that the scattering mechanisms discussed in this paper (mostly based on previous literature) are applicable for sigma-naught values (significantly dependent on polarization). Therefore, substantial justification should be provided on why beta-naught values are used. And if they are, how does the scattering mechanisms change?

A3: In the Methods section, it was incorrectly indicated that the TerraSAR-X data had been processed in beta-naught. The data is actually in the conventional sigma-naught, which is why the sigma symbol is used throughout the manuscript. Ice type classification was performed based on photograph interpretation (see R4 and answers).

M3: Corrected:

> *"This workflow starts with a conversion from the digital number to radar brightness (sigma-naught) [...]." (in the Methods)*

R4: c) The interesting part is how authors easily interpret different ice types (grease ice, nilas, pancake ice, and grey-white ice) without any geophysical explanation (or the least scattering mechanism) justifying the backscatter occurrence from these ice types. This needs to be clarified. Although the authors have demonstrated diversity in VV (figure 10) for different ice types, the authors should demonstrate the proof of how they classified or interpreted them as these 'specific' ice types.

A4: Ice type identification was performed based on photograph interpretation, by following the WMO nomenclature (WMO, 2014). Ice type backscattering signature was extracted by co-interpreting the photographs and satellite images. This has been clarified in the Methods. Specifically, grease ice, nilas, and pancake ice types were observed on the photographs. Since grey-white ice is essentially characterized by its thickness, we removed the identification of this type of ice and instead refer to ice less than two weeks old as "unidentified ice".

M4:

In the Methods, a section is reserved to describe remote sensing and photograph co-interpretation, with examples:

> *"TerraSAR-X images were interpreted spatially using coincident photographs taken from the shore. Observed features include open water areas or leads and different ice types. Figure 6 shows two examples. At the top, nilas, pancake ice and grease ice are observed on the photographs during the 2017 freeze-up process, and then identified on a coincident TerraSAR-X image from 26 November.*

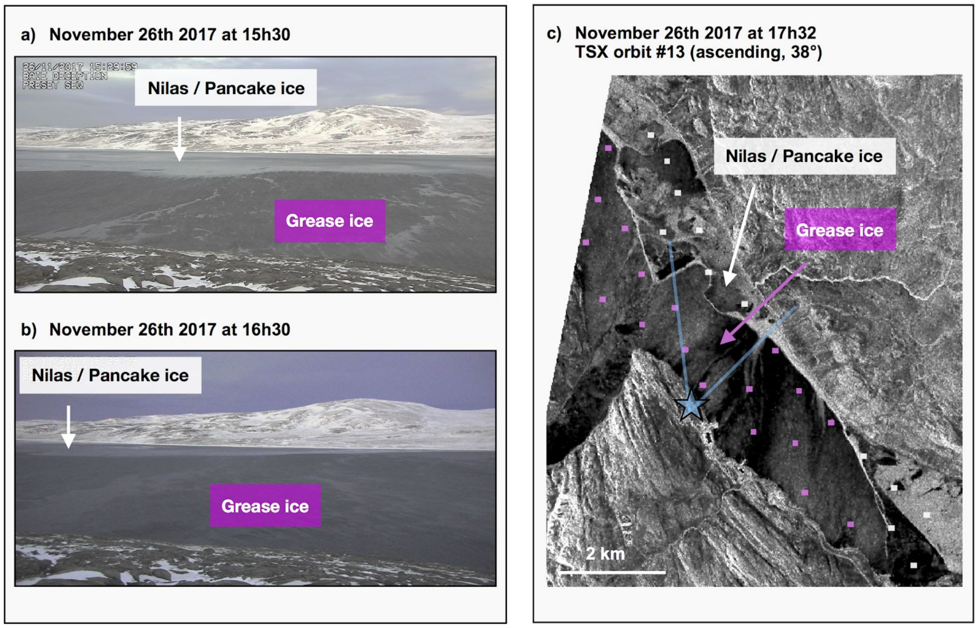

***Figure 6**: Coincident time-lapse photography and TerraSAR-X image during the 2017 freeze-up process. On the image, camera location and fields of view are identified in blue. The TerraSAR-X VV image, grey-scaled from -19 to -5 dB, is from orbit 13. AOIs are color-coded according to the identified ice type, prior to backscattering signature extraction.” (in the Methods)*

In the Results, backscattering data is presented for ice types identified from photographs and for unidentified young ice less than two weeks old:

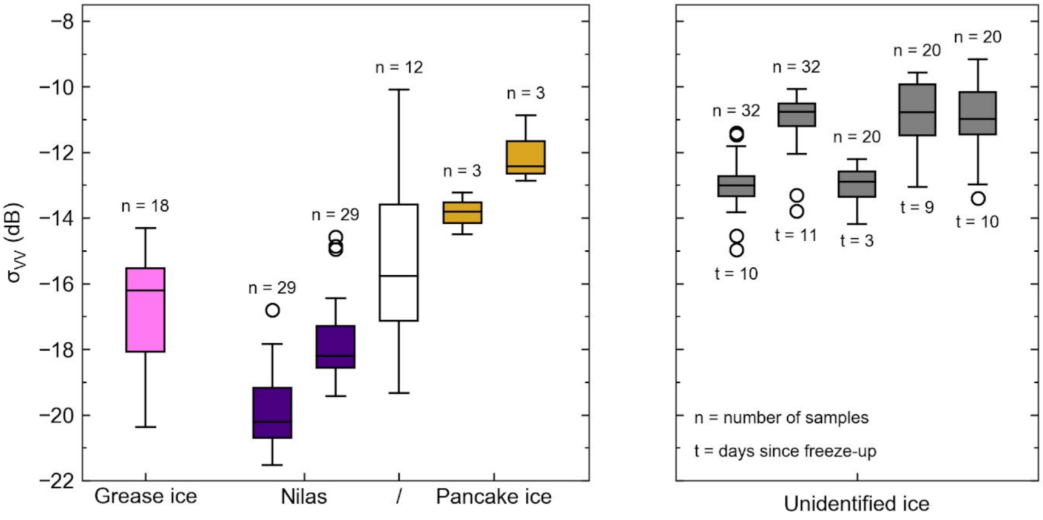

***Figure 8**: TerraSAR-X median VV backscattering values observed over AOIs of ice types identified from time-lapse photography in 2016 and 2017. The number of median values used (n) is written above each box. Outliers are plotted as empty white circles. Left: Grease ice (pink) was observed on the orbit 13 image from 26 November 2017. Nilas (dark purple) was observed on 28 and 29 November 2016 in orbits 13 and 21,*

respectively. A mix of nilas and pancake ice (white) was observed on 26 November 2017 in orbit 13. Pancake ice (yellow) was observed on 28 and 29 November 2016 in orbits 13 and 21. Right: Unidentified young ice (grey) was observed on 9 and 10 December 2016 in orbits 13 and 21, as well as on 1, 7 and 8 December 2017 in orbits 89, 13, and 21. The number of days since the freeze-up date (t) is written below each box. (in the Results)

R5: For another example, the authors talk about ’frost flower maximum’ which causes the first X-band inflection point. But the authors do not provide any proof of frost flower formation.
A5: We agree that the post-freeze-up peak cannot be reliably attributed to the presence of frost flowers. Indeed, frost flowers are too small to be resolved on the photographs.
M5: As described in our answer to R1 (above), association of seasonal features (e.g. post-freeze-up peak) to physical processes and scattering mechanisms has been removed from the Methods and Results, and is instead reserved for the Discussion, when possible.

R5: d) The third missing point of this paper is the lack of scattering mechanism explanation (mostly assumptions and backing up from past literature on C-band now) or sometimes explaining without any clarity in this regard. The authors should explain what they observe from the VV backscatter, based on the incidence angle range used in this study (and if they have in situ observations of snow and sea ice properties) and NOT based on agreeing with that they see from the SAR imagery, against past literature (using different incidence angle ranges from C-band imagery).
A5: Following your comments and those of Referee #2, we added some discussion on the effect of the incidence angle range used in the study. In the absence of in situ observations (given the focus of this paper on the combined use of two remote observation tools), definitive explanation of the scattering mechanisms is not possible. We however provide hypotheses for the mechanisms responsible for the seasonal features, which are more or less involved depending on the available literature (e.g. it is harder to speculate on mechanisms causing the post-freeze-peak than on those associated with melting and ponding).
M5:
The discussion was rewritten and includes segments on the scattering mechanisms for each seasonal process (examples are M1, M6). To avoid the logical fallacies you identified in your comments (e.g. X-band = C-band, or “cause of C-band feature” = “cause of X-band feature”), they are structured as follows:

1. Description, from the results, of an X-band feature
2. Existence, from the literature, of a seasonnaly coincident similar feature in the C-band (ex. inflexion point, peak)
3. Description, from the literature, of scattering mechanisms and snow or sea ice processes explaining this C-band feature
4. Discussion, from speculation, on how these mechanisms may translate or not to the X-band, in the event of these snow or sea ice processes

Added a discussion on incidence angle:

> *"Before moving on to the spring processes, we first discuss the influence of an 8° difference between ascending orbits 13 and 89. For 2016-2017 and 2017-2018, a small incidence angle effect was seen during the post-freeze-up and spring peaks, where backscattering was 1 to 3 dB smaller at the higher incidence angle, and no effect was seen during the monotone winter period (see Fig. 9 and 12). A backscattering signal which decreases with incidence angle is expected for situations dominated by surface scattering on a relatively rough surface (Ulaby et al., 1986). In the C-band, surface scattering at the interfaces between dry snow, brine-wetted snow and ice is indeed expected to dominate for cold snow-covered sea ice, with a transition to mixed scattering for thicker snow covers (Gill et al., 2015). We speculate that surface scattering on the ice formed from nilas patches explains the dependence on incidence angle observed in our X-band data. 2015-2016 however presents a very different case. Backscattering at the higher incidence angle is consistently 2 dB stronger than at the lower incidence angle, throughout winter and during the spring peak (see Fig. 12). We've shown the freeze-up process to have been different that year compared to 2016 and 2017, and already suggested that the ice cover was much smoother for the 2015-2016 season. We speculate that surface scattering was consistently low that year, and that volume scattering, which Ulaby et al. (1986) have shown can increase with incidence angle, dominated instead." (in the Discussion)*

R6: e) If the authors haven't noticed, one advantage of the X-band signature time series across three years is its utility to detect melt and pond onset from SAR images (which is always challenging) and how varied the dates are for these three years. The authors, if interested should consider using this application as a tool to improve this manuscript. In addition to freeze-up and break up, another application in which the science community and also local communities are interested in how the timing of melt and ponding changes and how it can be effectively detected from SAR images. Just a suggestion for improvement.

A6: A discussion on the mechanisms which may reasonably explain the link between spring features (end of monotone backscattering and spring peak) and spring processes (melt onset and pond onset) has been added.

M6:

The end of monotone backscattering in the X-band was explained as follows:

> *"Monotone X-band backscattering was observed every winter of the study, for all incidence angles and acquisition times, before a systematic springtime increase in backscattering. In the C-band, monotone backscattering is also observed in the winter, ending with melt onset brought on by warmer air temperatures (Yackel et al., 2007). Mechanisms which may increase C-band backscattering from snow-covered sea ice include surface scattering from the brine-wetted layer at the bottom of the snowpack (Nandan et al., 2016), volume scattering on brine inclusions enlarged by an increase in temperature (Barber and Nghiem, 1999), and surface scattering on wet snow (Gill et al., 2015; Yackel et al., 2007) accumulated at the top of the snowpack due to above-zero temperatures and solar radiation (Gogineni et al., 1992; Kim et al., 1984). We speculate that the X-band is susceptible to all of these C-band mechanisms, with*

> *an emphasis on surface scattering due to its lower penetration depth (Nandan et al., 2016), and attribute the end of X-band monotone backscattering to melt onset." (in the Discussion)*

The spring peak in the X-band was explained as follows:

> *"Springtime backscattering was seen to eventually peak in all TerraSAR-X datasets (Fig. 12), although one series featured more than one maximum (orbit 13, 2015-2016), another none (orbit 13, 2017-2018), and an apparent mismatch between maximum location in the 2015-2016 data. In the C-band, springtime peaking of the backscattering is attributed (Yackel et al., 2007; Barber et al., 1995) to the transition from the pendular regime, where water is held in the snowpack (Scharien et al., 2012), to the funicular regime where meltwater drains downward (Scharien et al., 2012), flushing out brine (Barber et al., 1995), and potentially refreezing (Gogineni et al., 1992). Mechanisms which may decrease the C-band backscattering following this transition are attributed to a decrease in the dielectric properties of the snowpack following water drainage (Yackel et al., 2007). We speculate that the decrease in the X-band springtime backscattering is also caused by pond onset, and associated with increased penetration in the snowpack after water has drained out of it." (in the Discussion)*

R7: Overall, if the authors would like to stick with the objective to provide a baseline understanding of X-band signature evolution, here are my suggestions

a) Even though data for all three years are available, use signatures from one year as the baseline and study the evolution of the X-band signature. That would be your baseline (which should also include describing the X-band scattering mechanisms).

b) With lack of in situ snow and sea ice observations of geophysical properties, the authors have the freedom to speculate the scattering mechanisms (never a drawback, and always room for improvements) instead of blind conviction.

c) Once the baseline signature is explained for one season, use it to differentiate different core regimes changes in the region. For eg. Table 3 shows differences in winter onset, melt onset and pond onset from SAR images for all three years. Use this info as a strong point to showcase the utility of X-band to effectively detect these changes (which can be then integrated into talking about the importance for local communities).

d) Use time-lapse photographs more as an ancillary data to explain the X-band signature evolution, and not the other way. Remember what your primary objective is.

A7: As described in A2, we chose to focus on the objective of combining TerraSAR-X and time-lapse photography time-series for seasonal monitoring of sea ice processes. The focus is therefore now less on the seasonal evolution of the X-band signal from sea ice, but rather on sea ice process monitoring through a combination of the two data sources.

The language was adapted throughout the manuscript to remove assumptions regarding scattering mechanisms and instead provide hypothetical explanations (see examples in M5 and M6).

M7: See M2, M5 and M6.

References

Barber, D. G. and Nghiem, S. V.: The role of snow on the thermal dependence of microwave backscatter over sea ice, J. Geophys. Res.-Oceans, 104(C11), 25789–25803, https://doi.org/10.1029/1999JC900181, 1999.

Barber, D. G., Papakyriakou, T. N., Ledrew, E. F. and Shokr, M. E.: An examination of the relation between the spring period evolution of the scattering coefficient (σ) and radiative fluxes over Jandfast sea-ice, Int. J. Remote Sens., 16(17), 3343–3363, https://doi.org/10.1080/01431169508954634, 1995.

Gill, J. P. S., Yackel, J. J., Geldsetzer, T. and Fuller, M. C.: Sensitivity of C-band synthetic aperture radar polarimetric parameters to snow thickness over landfast smooth first-year sea ice, Remote Sens. Environ., 166, 34–49, https://doi.org/10.1016/j.rse.2015.06.005, 2015.

Gogineni, S. P., Moore, R. K., Grenfell, T. C., Barber, D., Digby, S. and Drinkwater, M.: The effects of freeze-up and melt processes on microwave signatures, in Microwave remote sensing of sea ice, Geophys. Monogr. vol. 68, edited by F. D. Carsey, pp. 329–341., Washington, DC, 1992.

Kim, Y.-S., Onstott, R. and Moore, R.: Effect of a snow cover on microwave backscatter from sea ice, IEEE J. Oceanic Eng., 9(5), 383–388, https://doi.org/10.1109/JOE.1984.1145649, 1984.

Nandan, V., Geldsetzer, T., Islam, T., Yackel, John. J., Gill, J. P. S., Fuller, Mark. C., Gunn, G. and Duguay, C.: Ku-, X- and C-band measured and modeled microwave backscatter from a highly saline snow cover on first-year sea ice, Remote Sens. Environ., 187, 62–75, https://doi.org/10.1016/j.rse.2016.10.004, 2016.

Scharien, R. K., Yackel, J. J., Barber, D. G., Asplin, M., Gupta, M. and Isleifson, D.: Geophysical controls on C band polarimetric backscatter from melt pond covered Arctic first-year sea ice: Assessment using high-resolution scatterometry, J. Geophys. Res.-Oceans, 117(C00G18), https://doi.org/10.1029/2011JC007353, 2012.

Ulaby, F. T., R. K. Moore, and A. K. Fung. 1986. Microwave Remote Sensing: Active and Passive. Vol. Volume 3-From theory to applications. United States: Addison-Wesley Publishing Company. https://ntrs.nasa.gov/search.jsp?R=19860041708.

WMO: Sea-Ice Nomenclature, No. 259, World Meteorological Organization, Switzerland, 2014.

Yackel, J. J., Barber, D. G., Papakyriakou, T. N. and Breneman, C.: First-year sea ice spring melt transitions in the Canadian Arctic Archipelago from time-series synthetic aperture radar data, 1992–2002, Hydrol. Process., 21(2), 253–265, https://doi.org/10.1002/hyp.6240, 2007.

Dear **Referee #2**,

Thank you for your insightful comments on manuscript tc-2019-199 “Seasonal timeline for snow-covered sea ice processes in Nunavik's Deception Bay from TerraSAR-X and time-lapse photography.” and for providing advice on how to improve it. We appreciate your time. The manuscript has been considerably reworked following your comments and those of Referee #1.

The title and objectives have been reworded to reflect our focus on the combined use of TerraSAR-X and time-lapse photography for seasonal sea ice processes monitoring. Section 2. “SAR backscattering from sea ice” has been removed. The methods and results have been re-organized, and some content has been moved to the supplementary materials. The discussion has been completely rewritten.

We reproduced your comments below (R), provided our answers (A), and detailed changes to the manuscript (M). When providing section numbers, we refer to the first version of the manuscript.

Sophie Dufour-Beauséjour, for the authors
sophie.dufour-beausejour@ete.inrs.ca

R1: The abstract is rather imprecise, e.g. it is claimed that Inuit’s have reported greater inter-annual variability in the seasonal ice conditions. In which way were there changes? Since when have they reported this? This information is very useful and it would have been very nice if these observations were further reported and explored within the manuscript. Why can we expect increase in solid precipitation? Over which time period? Please rewrite the abstract to focus on the main findings and points addressed within the manuscript.

A1: The abstract was rewritten to focus on the main points addressed in the manuscript.

M1:

We added examples of changes to seasonal sea ice conditions reported by Inuit:

> *“Indeed, Inuit have reported greater inter-annual variability in seasonal sea ice conditions, including later freeze-up and earlier breakup.” (in the Abstract)*

Regarding climate projections, we clarified the information:

> *“The evolution of seasonal sea ice conditions in Deception Bay is expected to continue, with 2040-2064 climate projections for the region showing shorter snow cover periods and warmer annual average temperature (Mailhot and Chaumont, 2017).” (in the Introduction)*

R2: The manuscript is very long and contain information that is well covered in other works, e.g. the sea ice evolution during the year. Please reference these works instead, and only highlight things of specific importance and relevant to the scientific work carried out within this manuscript. This would significantly shorten the manuscript, e.g. can section 2 be significantly shortened to possibly cover 1/2 page instead of the near 3 pages. The study area section can also be shortened, e.g. is the tidal range is not important for the rest of the study. Similarly, is the last paragraph in section 3 not relevant for the presented work? Please revise the work bearing in mind what you are trying to convey and new scientific findings.

A2: The literature review on SAR backscattering from sea ice was shortened: highlights relevant for the manuscript were incorporated in the Introduction and in the Discussion. This, as well as the transfer of some content to the supplementary materials (as detailed in A11), has significantly shortened the manuscript.

M2:

Section “2. SAR backscattering over snow-covered sea ice”, which presented a literature review on the seasonal evolution of C-band backscattering from first-year sea ice, was removed following your comments as well as those of Referee #1. Relevant references to the literature on this topic are now reserved for the discussion.

Information on the tidal range was removed from Section “3. Study area”.

The paragraph detailing how the relevant local authorities were consulted and gave their approval for the project is still in the manuscript, because this information serves to demonstrate that the data was acquired in a respectful manner

R3: Please expand the methods section to explain to the reader what is done in the study and how the results are achieved. E.g. define and explain why the following is calculated; first freezing degree-day, freeze-up, frost flower maximum and winter onset?

A3: The methods section was expanded to include examples and definitions, and restructured to follow the manuscript objectives.

M3:

A paragraph explaining how the methods relate to the objectives of the manuscript was added as an introduction to the methods section:

> *“The objective of combining TerraSAR-X and time-lapse photography time-series for seasonal sea ice process observation is addressed by identifying indicators relating to freeze-up, winter, and breakup process elements. [...] Sections 4.1 and 4.2 describe the indicators and how they are observed or measured from each data source. Section 4.3 then explains how photographs are compared with coincident satellite images and used to identify their features, which serves to evaluate the potential of time-lapse photography to support TerraSAR-X image interpretation.*

In the Methods, we justify why each indicator is calculated by relating it to a process element, which is itself related to a given sea ice process:

> *“For example, elements of the freeze-up process include the date on which freeze-up begins, and the day on which it ends. These process elements can be observed through time-lapse photography indicators consisting of the first day where parts of the winter ice cover are observed on the water, and the first day where the winter ice cover is complete and stable.”*

R4: According to the manuscript frost flowers could not be observed in the photographs, and as far as the reader can work out a peak in SAR backscatter values is therefore inferred to correspond to frost flowers. Though this is not again specifically stated in the methods section.

Moreover, how do you know that frost flowers were present? Could the post-freeze-up peak be related to increased sea ice thickness?

A4: We agree that the post-freeze-up peak cannot be reliably attributed to the presence of frost flowers. Indeed, frost flowers are too small to be resolved on the photographs. In general, following your comments and those of Referee #1, we now refrain from associating X-band backscattering time-series features to sea ice processes (e.g. frost flowers). Instead, the features are tracked as they are (e.g. post-freeze-up peak) throughout the Methods and Results. Potential explanations for the features based on physical processes (e.g. frost flowers, or increased sea ice thickness) are now reserved for the Discussion.

The difference between our observations of backscattering from nilas and those of the literature, which are several dBs lower, is suggested to be caused by the presence of a snow cover (snowfall was observed on the photographs). Frost flowers are cited as a possible additional source of scattering which cannot be resolved on the photographs (see excerpt below in M4). Regarding the specific case of the post-freeze-up peak, we were unable to confidently associate it with a physical process such as the presence of frost flowers or the growth of ice thickness, because of the relative lack of literature on X-band backscattering mechanisms within sea ice, particularly young sea ice in the winter. We do however offer potential explanations in the Discussion (see excerpt below in M4).

M4:

On the role frost flowers may have played in backscattering from nilas:

> *"In cold and dry snow conditions, the X-band isn't expected to penetrate significantly in the ice cover, with backscattering dominated by the presence of brine at the snow-ice interface (Nandan et al., 2016). Several factors may be intervening in backscattering from nilas. Frost flowers are known to increase the backscattering from newly formed sea ice in the C-band, an effect which may be more pronounced over thin ice; an increase of 5 dB was reported over ice 2 to 15 cm thick (Nghiem et al., 1997), and of 13 dB over 5 cm thick ice (Isleifson et al., 2014). Snow may also lead to an increase in backscattering through warming of the ice surface and brine absorption (Gill et al., 2015). In the case of our nilas observations, snow itself might be enough to explain the 3 dB difference; frost flowers may also have played a role, but cannot be observed on the photographs." (in the Discussion)*

On the mechanisms responsible for the post-freeze-up peak:

> *"The post-freeze-up peak and monotone backscattering onset are also observed in C-band time-series over sea ice (Yackel et al., 2007), but these seasonal features have been less studied than their spring counterparts (end of monotone backscattering and spring peak). Moreover, the same features in the X and C-band could well be related to different scattering mechanisms, and even to different physical processes. We limit ourselves to speculating, for the X-band data presented in this manuscript, that the increasing portion of the peak may be associated with the domination of surface scattering related to a brine-rich ice surface, potentially covered in frost flower, and that the decreasing portion may be associated with a transition to*

> *an absorption regime, in which the signal suffers loss in the brine-wetted and increasingly colder snow. " (in the Discussion)*

R5: Why are not snow thickness information reported for any other time period than April 2017? In order to fully address the scientific topic indicated in the title of the paper information about the snow thickness is essential for the sea ice monitoring. It is unclear to the reader how are the estimates about the snow cover carried out? Photographs? Is there information about snow cover thickness and distribution? Judging by the title the manuscript should only contain information about snow-covered sea ice. Yet figures showing e.g., grease ice and pancake ice has no snow cover. Consider updating the title to reflect the sea ice included within the study. Please discus how do you expect the snow-cover to affect the results?
A5: The title of the manuscript and its objectives were reworded to better reflect the manuscript's focus on the combined use of TerraSAR-X and time-lapse photography for seasonal sea ice processes monitoring. Snow thickness measurements, performed by the authors as part of the greater Ice Monitoring project and included as context for the study site, have been updated to the entire available range of data (2015 to 2018).

The presence of a snow cover on the sea ice, which is the case for almost all the TerraSAR-X images in the time-series, is expected to play a significant role in the total backscattering and its seasonal evolution. Following freeze-up, the snow absorbs brine expelled from the new ice (Barber and Nghiem, 1999). The presence of brine in the snow is expected to restrain the interaction of the signal to the snow volume and the snow-ice surface because of absorption in the lossy brine-wetted snow (Nandan et al., 2016). Penetration in the ice cover itself is therefore small (modelled penetration depth is for the X-band VV is 2 cm in brine-wetted snow, as reported by Nandan et al., 2016). Relevant scattering mechanisms should be limited to surface and volume scattering within the snow layers and surface scattering at the snow-ice interface.
M5:
Reworded Title:

> *"Combining TerraSAR-X and time-lapse photography for seasonal sea ice monitoring: the case of Deception Bay, Nunavik" (Title)*

Reworded manuscript objectives:

> *"This article explores the use of combined TerraSAR-X and time-lapse photography time-series to observe seasonal sea ice processes, and the potential of the time-lapse photography to support TerraSAR-X interpretation. The case study is performed over three years in Nunavik's Deception Bay. A complementary objective is to describe the processes through an interannual comparison. (in the Introduction)*

Updated snow thickness data and provided details and a reference regarding the measurement method:

> *"Point thickness measurements performed in Deception Bay for the Ice Monitoring project in January-February and April-May 2016, 2017, and 2018 (Gauthier et al., 2018) ranged from 0 to 55 cm for the snow cover, and 52 to 165 cm for the ice cover. " (in the Study area)*

R6: Why is beta nought used instead of the more commonly used sigma nought? Since beta nought is used please use the symbol beta in all the figures 6, 10, 11, 12 and 16 instead of the symbol sigma.

A6: In the Methods section, it was incorrectly indicated that the TerraSAR-X data had been processed in beta-naught. The data is actually in the conventional sigma-naught, which is why the sigma symbol is used throughout the manuscript.

M6: Corrected:

> *"This workflow starts with a conversion from the digital number to radar brightness (sigma-naught) [...]." (in the Methods)*

R7: The incidence angle difference within the dataset is significant (8o), how does this affect the presented results?

A7: The seasonal features (peaks and inflexion points) were observed for all acquisition parameters, so the different incidence angles between orbits doesn't affect the results presented in the manuscript. The relative amplitude of the features did however sometimes depended on incidence angle. To discuss the effect of incidence angle, we compare the two ascending-evening orbits. Orbit 13 (empty squares) at an incidence angle of 38° and orbit 89 (black diamonds) at an incidence angle of 46° are first shown for 2017-2018 (see Fig. R2-1).

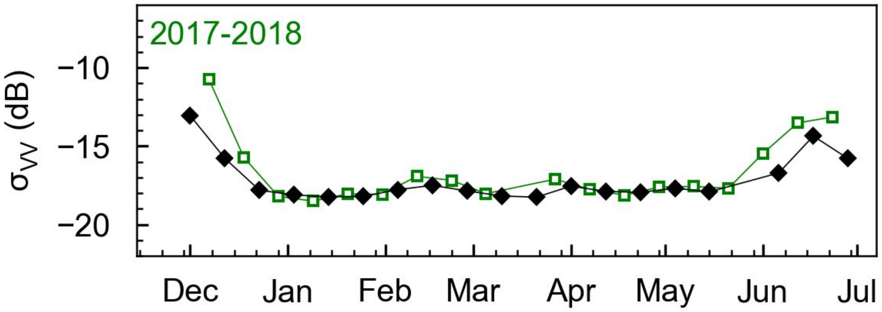

Figure R2-1: TerraSAR-X median VV backscattering plotted versus time for 2017-2018. Two orbits are shown: orbits 13 (38°, empty square) and 89 (46°, black diamond).

A small incidence angle effect can be seen on the median VV backscattering during the post-freeze-up and spring peaks. The backscattering at 38° is 1 to 3 dB higher than the backscattering at 46°. No incidence angle effect is seen in the monotone winter period. The same is observed in 2016-2017 (see Fig. R2-2). A backscattering signal which decreases with incidence angle is expected for situations dominated by surface scattering on a relatively rough surface (Ulaby et al., 1986). Surface scattering at the interfaces between dry snow, brine-wetted snow and ice is indeed expected to dominate backscattering from cold snow-covered sea ice, with a transition to mixed scattering for thicker snow covers (Gill et al., 2015). The monotone winter period where no incidence angle effect is observed might be associated with mixed scattering.

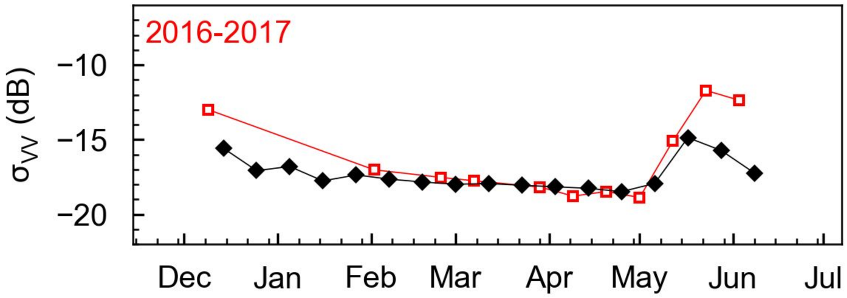

Figure R2-2: TerraSAR-X median VV backscattering plotted versus time for 2016-2017. Two orbits are shown: orbits 13 (38°, empty square) and 89 (46°, black diamond).

The effect of incidence angle is completely different in 2015-2016 however. There is an almost constant difference of 2 dB between the two orbits, with the backscattering at 38° always **lower** than the 46° backscattering (see Fig. R2-3). The freeze-up process was also different in 2015: the thermal freeze-up is expected to have produced smooth thermal ice, compared to rougher ice from nilas patches and other ice types in 2016 and 2017. We suggest that, for 2015-2016, the surface scattering at the snow-ice interface was consistently low because of a smoother ice cover, and that the total backscattering was dominated instead by volume scattering. Volume scattering may increase with incidence angle (Ulaby et al., 1986), as observed in the 2015-2016 data throughout the winter and spring.

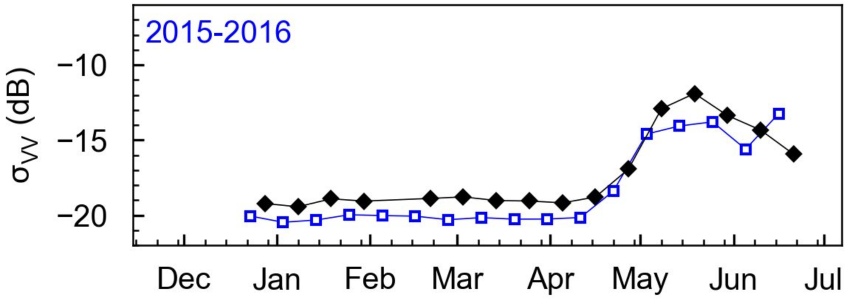

Figure R2-3: TerraSAR-X median VV backscattering plotted versus time for 2015-2016. Two orbits are shown: orbits 13 (38°, empty square) and 89 (46°, black diamond).

M7: A discussion on the effect of incidence angle has been added to the discussion:

> *"Before moving on to the spring processes, we first discuss the influence of an 8° difference between ascending orbits 13 and 89. For 2016-2017 and 2017-2018, a small incidence angle effect was seen during the post-freeze-up and spring peaks, where backscattering was 1 to 3 dB smaller at the higher incidence angle, and no effect was seen during the monotone winter period (see Fig. 9 and 12). A backscattering signal which decreases with incidence angle is expected for situations dominated by surface scattering on a relatively rough surface (Ulaby et al., 1986). In the C-band, surface scattering at the interfaces between dry snow, brine-wetted snow and ice is indeed expected to dominate for cold snow-covered sea ice, with a transition*

> *to mixed scattering for thicker snow covers (Gill et al., 2015). We speculate that surface scattering on the ice formed from nilas patches explains the dependence on incidence angle observed in our X-band data. 2015-2016 however presents a very different case. Backscattering at the higher incidence angle is consistently 2 dB stronger than at the lower incidence angle, throughout winter and during the spring peak (see Fig. 12). We've shown the freeze-up process to have been different that year compared to 2016 and 2017, and already suggested that the ice cover was much smoother for the 2015-2016 season. We speculate that surface scattering was consistently low that year, and that volume scattering, which Ulaby et al. (1986) have shown can increase with incidence angle, dominated instead." (in the Discussion)*

R8: The fjord is given as 20 km wide (a scale bar would be nice to see in Figure 2), how much of the overall area is covered by the 15km wide TerraSAR-X images?

A8: A scale bar was added to Fig. 2, and the overlap between the study area and the TerraSAR-X image subset (a 9 km long section of the bay) is now indicated in the description of the study site and the TerraSAR-X data.

M8:

Added a scale bar to the map of Deception Bay.

Added detail on study area coverage by the TerraSAR-X images:

> *"Figure 2 shows the extent of the subimages, which overlaps with a 9 km long section of the bay." (in Data description)*

R9: It is in the discussion stated that the sea ice observed in the ship wake was broken. How is this verified? How are wind effects accounted for in these observations? Would it be possible to include observations from these ships?

A9: Following their transit in the bay, the *MV Nunavik* and *MV Arctic* leave a track of open water and floating broken ice pieces. Because the ice cover is landfast to both shores, the track remains "open" until it has refrozen (in the winter); it is never closed by wind or currents. Ice lateral movement under the effect of the wind could be resolved on time-lapse photography, and was not observed. The refreezing of the track will depend on how much broken ice is in the open water and on the air temperature. The broken ice left in the ship's wake can be observed on time-lapse photography for the areas close to the cameras. We also observed the tracks left by the ships during winter fieldwork in Deception Bay in 2016, 2017, and 2018. During the spring, when ice-breaking transport resumes around June 1st, the tracks left by the ship are unlikely to refreeze due to warm temperatures. We speculate that the ship tracks are then left open, potentially with floating ice pieces depending on the ice and meteorological conditions. We don't have access to observations from the ships.

M9: Following the rewrite, the particular sentence which referred to broken ice left in the ship's wake is no longer in the discussion.

The effect of the wind (or absence thereof) has been added to the discussion on breakup processes:

> *"We speculate that the ice cover was in a more advanced state of degradation when breakup started in 2016 than in 2017. This is supported by time-lapse photography*

which show that the ice cover was partly mobile (under the effect of wind or current) during breakup 2016, but mostly landfast during breakup 2017 (Movies S4-S5). In 2018's comparatively late spring, both the MV Nunavik and MV Arctic entered the bay during pond onset (on June 17th). Open water was observed along their tracks in the following days, and new cracks perpendicular to the shore appeared when the ships left the bay eight days later." (in the Discussion)

R10: It is in the manuscript stated that the X-band backscatter change is expected to be similar to the one in C-band. A suggested to corroborate this is to include Sentinel-1 images overlapping the fjord to investigate if these C-band images show the same evolution as the TerraSAR-X images. The use of Sentinel-1 may also reduce the revisit time.
A10: Following comments from Referee #1, we removed the assumption that the seasonal evolution of the X-band backscattering should be similar to that of the C-band. The question of similarity between the two bands is now reserved for the discussion.

During the Ice Monitoring project, RADARSAT-2 C-band data was acquired during winters (December to April) 2015-2016, 2016-2017, and 2017-2018, in partnership with the Canadian Ice Service. The median VV RADARSAT-2 backscattering at 36° over the same AOIs as presented in the paper is shown in Fig. R2-4, alongside TerraSAR-X data from orbit 13 at 38°. The RADARSAT-2 data was processed in the same way as the TerraSAR-X data, using the Multi-SAR-System at DLR.

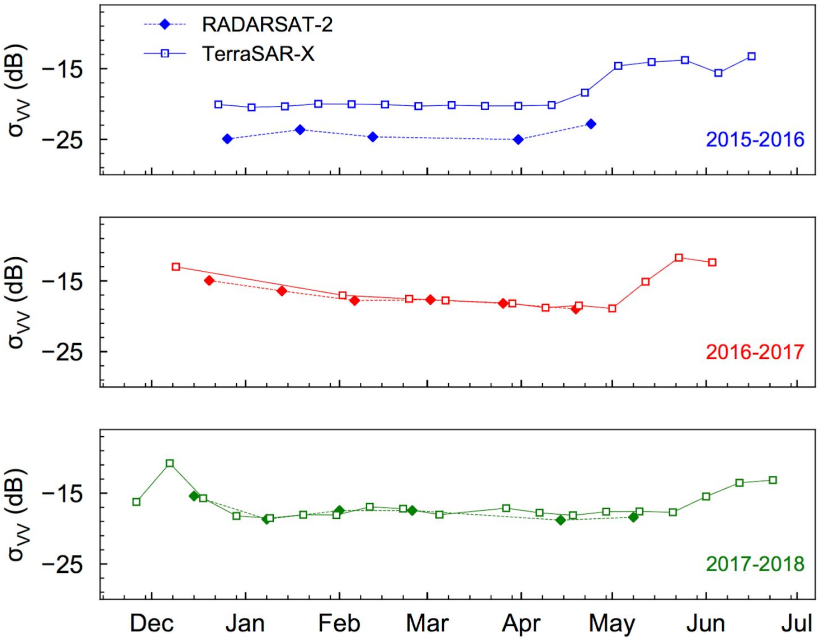

Figure R2-4: TerraSAR-X (38°) and RADARSAT-2 (36°) median VV backscattering plotted versus time. RADARSAT-2: in full diamonds and TerraSAR-X in empty squares.

The available RADARSAT-2 data closely matches the TerraSAR-X time-series for 2016-2017 and 2017-2018 monotone winter periods, as well as for the 2017 acquisition in the post-freeze-up peak. No data is available during one of the spring peaks. In 2015-2016, the monotone winter period backscattering is consistently lower in the C-band than in the X-band, by approximately 4 dB, which is probably due to differences in penetration depth. As described in A7, ice in 2015-2016 was presumably smoother than the other two years. The low signal both in X and C-band (Fig. R2-4) suggests that the ice appeared smooth at both radar frequencies. The C-band's increased penetration depth (due to a longer wavelength) might have led to increased absorption of the signal by brine inclusions in the sea ice, leading to a lower total backscattering than at the X-band.

M10: Added to the conclusion:

> *"Future work in the Ice Monitoring project will build on this characterization of seasonal processes and focus on spatial variations within the bay and comparison with similar fjords, namely Salluit and Kangiqsujuaq. It will also involve comparison of the TerraSAR-X time-series data with RADARSAT-2 time-series acquired over the same period and area." (in the Conclusion)*

R11: Rather than stating that the standard meteorological station at the airport is not used, a correlation measure between the used temperature and the airport temperature would have been beneficial. Such a comparison would also have verified the supposedly heated camera case claim, rather than a statement that the authors think that it is so. At what altitude is the temperature sensor located?

A11: We performed a correlation analysis between the camera temperature measured in Deception Bay and the airport temperature measured in Salluit, 50 km away. Everything related to the temperature measurements has been moved to a supplementary document focused on air temperature. It includes a description of the two different temperature data sources (including altitude), the data acquisition method, and a comparison of the two datasets (including the Pearson coefficient). The airport data was shown to be strongly correlated to the Deception Bay camera measurement. We therefore chose to use the airport data, despite the 50 km distance, to document how warm or cold each month was. We removed the bias modeling and correction for the camera data. Results on monthly cumulative freezing and thawing degree-days are given in the supplementary document for the airport dataset, and cited at several points in the Discussion.

M11:

Added detail to the description of the temperature data:

> *"The closest weather station to Deception Bay is located in neighboring Salluit, at the airport. Measurements at the station are taken hourly during the day, and their daily mean is available online from Environment Canada. Salluit is a Nunavik coastal community located 50 km west of Deception Bay; the airport is located 2.8 km inland at an altitude of 226 m.*
>
> *Two Reconyx PC800 Hyperfire Professional Semi Covert cameras were installed in Deception Bay as part of the CAIMAN research project. These cameras were installed*

> *near the study area, in front of Moosehead Island at an altitude of 22 m (series A) and on Black Point at an altitude of 33 m (series B)." (in the Supplementary)*

Added a correlation analysis:

> *"Figure S3-2 shows the camera and airport datasets from 2015 to 2018. The camera and airport measurements showed a Pearson coefficient of 0.98 and 0.99 for the three years of the study, which proves a strong correlation despite their different locations. The camera dataset however differs from the airport's dataset with a root mean-squared-error (RMSE) of 3.9 to 4.3°C. To investigate this discrepancy, Fig. S3-2 also shows that the daily difference between the two datasets is roughly flat from September to January, and then peaks in April-May.*

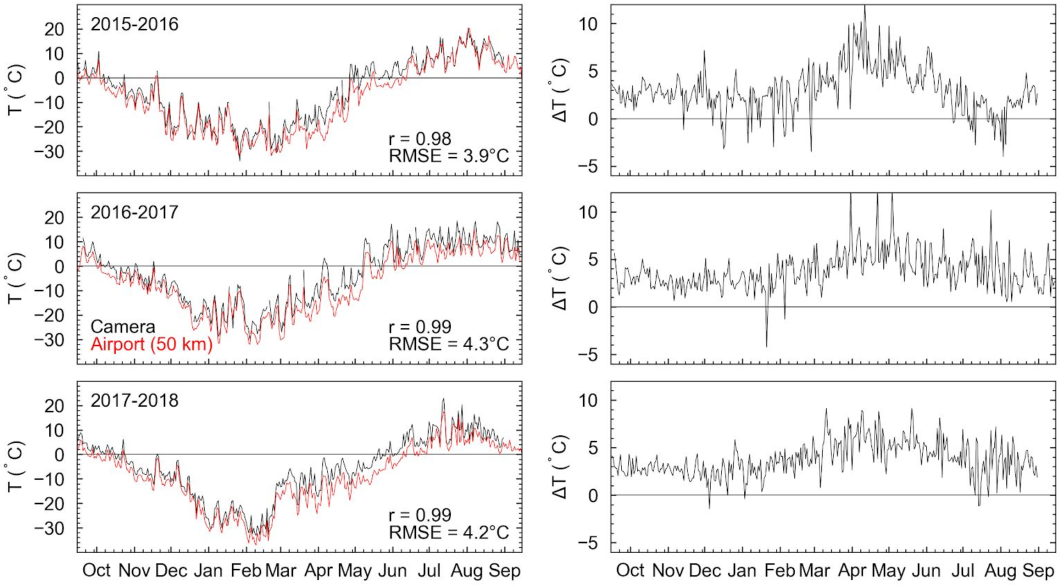

> ***Figure S3-2**: Left: Daily mean air temperature measured by the camera in Deception Bay (black) and at the Salluit airport (red). Right: Daily difference between the two datasets." (in the Supplementary)*

R12: As stated in the manuscript is FDD used, yet the unit used was oC, please explain? Also freezing at +3.5 oC to +4oC seems a bit high. Why is 0oC used when sea ice is investigated as it will likely freeze at -1.8oC. Are there any sea water temperature measurements?

A12: Freezing degree-days are a sum of temperatures (measured in °C). Since summation preserves units, FDDs were presented with a °C.

Freezing degree-days are a sum of freezing temperatures normalized to a positive number; freezing degree-days of 3.5 and 4.5 °C on average therefore mean that the daily temperature was roughly -4°C on average between the first freezing day of the year and the day of freeze-up, which is coherent with water freezing at -1.8°C.

While it is true that sea water freezes at slightly lower temperatures than fresh water, we chose to use the conventional definition of freezing and thawing degree-days (relative to the 0°C mark), used by the Ouranos consortium in their climate projections for the region for instance (Mailhot and Chaumont, 2017).

No surface sea water temperature measurements were made as part of the fieldwork for this project. Temperature measurements reported in the literature were taken in September 2006 (GENIVAR, 2007) and August 2012 (GENIVAR, 2012).

M12: Added the reference to the Ouranos consortium climate projections to the description of freezing and thawing degree-days.

R13: It is mentioned in the discussion that the Deception River has warm water, please provide a temperature time series for this river or at least give some specific temperatures.

A13: No water temperature measurements were performed for Deception River, and we found no such data in the literature for the breakup period.

M13: The statement on Deception River having warm or warmer water was removed from the discussion.

R14: How do the values in e.g. Fig. 10 relate to e.g. work by Onstott 1992?

A14: We added a comparison of our results with those presented by Onstott (1992) and others.

M14: Added:

> *“Despite a difference of almost 20° in the incidence angle, our observation of -12 ± 1 dB over unidentified ice one to nine days after freeze-up (Fig. 8) is close to [...] reports by Onstott (1992) of -14.4 dB over thin first year ice (30 to 70 cm thick) in the X-band HH at 23°.” (in the Discussion)*

R15: Additional comments According to the temperature records, as presented on row 254, temperatures are recorded between 11 September 2015 – 16 September 2016 and then from 18 September 2018 (?) to 31 August 2018. Please clarify.

A15: This is a mistake; the correct date ranges are 11 September 2015 – 16 September 2016 and 18 September 2016 – 31 August 2018.

M15: Corrected in the manuscript.

R16: Ibid. is not a way to reference that I’ve seen in this journal before. Whilst this might still be ok, many of the references where ibid. has been used are not correct and the statements that are supposed to be covered in those references are not included here. E.g. on row 129 the “white ice” term is attributed to Johansson et. al., 2017 and on row 400 correctly to WMO. Moreover, when referring to the WMO terminology please include the full reference, (WMO, 2014).

A16: We removed all uses of “ibid” and checked all citations.

M16: All uses of “ibid” were changed to in-text citations.

References

Barber, D. G. and Nghiem, S. V.: The role of snow on the thermal dependence of microwave backscatter over sea ice, J. Geophys. Res.-Oceans, 104(C11), 25789–25803, https://doi.org/10.1029/1999JC900181, 1999.

Gauthier, Y., Dufour-Beauséjour, S., Poulin, J., and Bernier, M. 2018. Ice Monitoring in Deception Bay : Progress report 2016-2018. Québec: INRS, Centre Eau Terre Environnement. http://espace.inrs.ca/7538/.

GENIVAR: Projet Nickélifère Raglan Sud – Rapport principal – Étude d'impact sur l'environnement et le milieu social. Rapport de GENIVAR Société en commandite pour Canadian Royalties inc. Montreal, Que.,2007.

GENIVAR: Environmental and Social Impact Assessment of the Deception Bay Wharf and Sediment Management, Report from GENIVAR for Canadian Royalties Inc., Montreal, Que., 2012.

Gill, J. P. S., Yackel, J. J., Geldsetzer, T. and Fuller, M. C.: Sensitivity of C-band synthetic aperture radar polarimetric parameters to snow thickness over landfast smooth first-year sea ice, Remote Sens. Environ., 166, 34–49, https://doi.org/10.1016/j.rse.2015.06.005, 2015.

Isleifson, D., Galley, R. J., Barber, D. G., Landy, J. C., Komarov, A. S. and Shafai, L.: A Study on the C-Band Polarimetric Scattering and Physical Characteristics of Frost Flowers on Experimental Sea Ice, IEEE Transactions on Geoscience and Remote Sensing, 52(3), 1787–1798, https://doi.org/10.1109/TGRS.2013.2255060, 2014.

Mailhot, A. and Chaumont, D.: Élaboration du portrait bioclimatique futur du Nunavik - Tome II. Rapport présenté au Ministère de la forêt, de la faune et des parcs., Ouranos, Montreal, Que., 2017.

Nandan, V., Geldsetzer, T., Islam, T., Yackel, John. J., Gill, J. P. S., Fuller, Mark. C., Gunn, G. and Duguay, C.: Ku-, X- and C-band measured and modeled microwave backscatter from a highly saline snow cover on first-year sea ice, Remote Sens. Environ., 187, 62–75, https://doi.org/10.1016/j.rse.2016.10.004, 2016.

Nghiem, S. V., S. Martin, D. K. Perovich, R. Kwok, R. Drucker, and A. J. Gow. 1997. “A Laboratory Study of the Effect of Frost Flowers on C Band Radar Backscatter from Sea Ice.” Journal of Geophysical Research: Oceans102 (C2): 3357–70. https://doi.org/10.1029/96JC03208.

Onstott, R. G.: SAR and Scatterometer Signatures of Sea Ice, in: Microwave Remote Sensing of Sea Ice, American Geophysical Union, Washington, D.C., United States, 73-104, 1992.

Ulaby, F. T., R. K. Moore, and A. K. Fung. 1986. Microwave Remote Sensing: Active and Passive. Vol. Volume 3-From theory to applications. United States: Addison-Wesley Publishing Company. https://ntrs.nasa.gov/search.jsp?R=19860041708.

Yackel, J. J., Barber, D. G., Papakyriakou, T. N. and Breneman, C.: First-year sea ice spring melt transitions in the Canadian Arctic Archipelago from time-series synthetic aperture radar data, 1992–2002, Hydrol. Process., 21(2), 253–265, https://doi.org/10.1002/hyp.6240, 2007.

List of changes

During major revisions, the following changes were made to manuscript tc-2019-199:

Title and abstract: The title was reworded and the abstract rewritten.

1. Introduction: The literature review on SAR was rewritten, as well as the objectives

(2. SAR backscattering from sea ice): This section from the original version was merged with the introduction and removed.

2. Study area: Some details were added.

3. Data description: The content related to air temperature measurements was moved to the supplementary materials.

4. Methods: This section was re-organized and rewritten. The methods relating to air temperature measurements were moved to the supplementary materials.

5. Results: Some details were added.

6. Discussion: The discussion was rewritten.

7. Conclusion: This section was rewritten.

Supplementary materials: Content on air temperature measurements was added, as well as movies showing TerraSAR-X time-series.

Sophie Dufour-Beauséjour, for the authors
sophie.dufour-beausejour@ete.inrs.ca

Combining TerraSAR-X and time-lapse photography for seasonal sea ice monitoring: the case of Deception Bay, Nunavik

Sophie Dufour-Beauséjour[1,2], Anna Wendleder[3], Yves Gauthier[1,2], Monique Bernier[1,2], Jimmy Poulin[1,2], Véronique Gilbert[4], Juupi Tuniq[5], Amélie Rouleau[6], Achim Roth[3]

[1]Centre Eau Terre Environnement, Institut national de la recherche scientifique (INRS), Quebec, G1K 9A9, Canada
[2]Centre d'études nordiques (CEN), Université Laval, Quebec, G1V 0A6, Canada
[3]German Aerospace Center (DLR), Oberpfaffenhofen, 82234 Weßling, Germany
[4]Kativik Regional Government, Kuujjuaq, J0M 1C0, Canada
[5]Salluit, J0M 1S0, Canada
[6]Raglan Mine (a Glencore Company), Laval, H7S 1Z5, Canada

Correspondence to: Sophie Dufour-Beauséjour (sophie.dufour-beausejour@ete.inrs.ca)

Abstract. This article presents a case study for the combined use of TerraSAR-X and time-lapse photography time-series in order to monitor seasonal sea ice processes in Nunavik's Deception Bay. This area is at the confluence of land use by local Inuit, ice-breaking transport by the mining industry, and climate change. Indeed, Inuit have reported greater inter-annual variability in seasonal sea ice conditions, including later freeze-up and earlier breakup. Time-series covering 2015 to 2018 were acquired for each data source: TerraSAR-X images were acquired every 11 days, and photographs hourly during the day. We used the combination of the two time-series to document spatio-temporal aspects of freeze-up and breakup processes. We also report new X-band backscattering values over newly formed sea ice types. The TerraSAR-X time-series further show potential for melt and pond onset.

1 Introduction

1.1 Context

Salluimiut (people of Salluit, Nunavik, in Canada) have reported changes in their environment, including less snow in the winter, which affects their activities on the land in Deception Bay (Tuniq et al., 2017). This area is prized by local Inuit for fishing as well as seal and caribou hunting (Petit et al., 2011). People from neighboring community Kangiqsujuaq have reported warmer and longer fall seasons, later freeze-up (Nickels et al., 2005), as well as less snow and earlier sea ice breakup in spring (Cuerrier et al., 2015). The evolution of seasonal sea ice conditions in Deception Bay should continue, with 2040-2064 climate projections for the region showing shorter snow cover periods and warmer annual average temperature (Mailhot and Chaumont, 2017). Further, two nickel mines have marine infrastructure in Deception Bay. Their ice-breakers transit in the bay from June 1st to mid-March, avoiding the seal reproduction period (GENIVAR, 2012). From January to March, Raglan Mine's *MV Arctic* performs on average two round-trips (Mussells et al., 2017). Local sea ice monitoring is relevant in light of local community members' reliance on the fjord's rich ecosystem for subsistence, as well as for shipping-related operations by the mines. More generally, this case study may be useful to those wishing to monitor seasonal processes in remote areas, or interested in sea ice processes.

1.2 Monitoring sea ice seasonal processes

First-year sea ice processes include, among others, formation through freeze-up, transformation of the snow and ice covers over the winter and spring, and eventual breakup. These processes may unfold differently from year to year due to meteorological conditions, over a period of time which may vary from a single day to weeks. They may be driven by environmental factors such as air temperature, wind, currents, and precipitation, to name several. The sequence of events may further depend on geomorphological features like shallows or deep water pockets, islands, and rivers. In order to document these seasonal processes, it is therefore necessary to rely both on spatial coverage of the bay as well as frequent observations. The combined use of radar remote sensing and time-lapse photography meets these requirements.

Synthetic aperture radar (SAR) sensors are uniquely qualified for winter applications in the polar regions: they can acquire images in the dark and through clouds. Modern options combine wide coverage and high spatial resolution with a revisit period as short as 11 days, in the case of TerraSAR-X (X-band, 9.65 GHz). SAR X-band has been shown to be a useful complement to the conventional C-band when it comes to first year sea ice: it was used to identify types of new ice (Johansson et al., 2017), particularly thin ice like nilas and grey ice (Matsuoka et al., 2001). The X-band is also reputed to be more sensitive to the snow cover and freeze/thaw processes than the C-band (Eriksson et al., 2010). Although the literature on X-band backscattering from first-year sea ice is sparse when compared to the C-band—two notable exceptions being Onstott (1992) and Nakamura et al. (2005)—several recent publications are bridging this gap. They include observations over new ice and nilas (Johansson et al., 2017; 2018) and white ice (Fors et al., 2016), as well as over first-year sea ice during the spring (Nandan et al. 2016; Paul et al., 2015). Recent studies have taken advantage of TerraSAR-X's frequent revisits to successfully document spatially extensive processes such as seasonal snow cover extent and snowmelt (Sobiech et al., 2012; Stettner et al., 2018), as well as glacier calving front monitoring (Zhang et al. 2019). In the C-band, a substantial ERS-1 and RADARSAT-1 (C-band, 5.405 GHz) time-series spanning 8 years was aggregated to study the springtime backscattering signature of snowmelt processes on first-year sea ice (Yackel et al., 2007).

Time-lapse photography is well suited for long-term monitoring applications related to the cryosphere: the systems can be installed in remote locations and record data as often as hourly, for prolonged periods of time. Such time-series have been used to track daily-to-seasonal variations in the extent of the sea ice and ice melange in front of a retreating glacier (Cassotto et al., 2015), to document glacier mass loss (Chauché et al., 2014) and albedo (Dumont et al. 2011), and to observe sea ice concentration in the Beaufort Sea (Wobus et al,. 2011). Time-lapse photography has also been used to document snow accumulation and accretion processes on mountain slopes (Vogel et al., 2012), snow cover extent in the tundra (Kepski et al.,

2017) and in forests (Arslan et al., 2017), as well as snow melt (Farinotti et al., 2010; Ide and Oguma, 2013; Peltoniemi et al., 2018; Revuelto et al., 2016). Bongio et al. (2019) successfully automated snow thickness measurements using time-lapse photography and measurement stakes in forestrial and alpine regions. Meteorological information may be derived from the photographs, for instance precipitation type or wind conditions (Christiansen, 2001; Liu et al., 2015; Smith Jr et al., 2003). Finally, Herdes et al. (2012) used sub-daily time-lapse photography time-series to validate and complement the visual interpretation of weekly RADARSAT-1 (C-band) time-series in the context of iceberg plumes and coincident sea ice conditions.

1.3 Objectives

This article explores the use of combined TerraSAR-X and time-lapse photography time-series to monitor seasonal sea ice processes, and the potential of the time-lapse photography to support TerraSAR-X interpretation. We performed this case study over three years in Nunavik's Deception Bay. A complementary objective is to describe the processes through an interannual comparison. This case study stands out due to the length of the time-series reported and its relevance to local actors.

Raglan Mine initiated this project in repsonse to local concerns about sea ice conditions in Deception Bay. The Northern Villages of Salluit and Kangiqsujuaq and both communities' Land Holding Corporations gave their approval for this project, including associated activities and instrumentation in Deception Bay. The Avataq Cultural Institute was consulted to ensure the project did not encroach on archaeological sites important to Inuit. Finally, the Nunavik Marine Region Impact Review Board gave permission for the deployment of underwater sonars in Deception Bay (sonar data not presented in this article).

2. Study area

Deception Bay (62° 09' N, 74° 40' W) is located on the northern edge of Nunavik, the Inuit Nunangat territory overlapping the Canadian province of Quebec north of the 55th parallel. This fjord of the Ungava Plateau is roughly 20 km long and nested in hills peaking at 580 m in altitude (GENIVAR, 2012). Water depth in the bay (Fig. 1) reaches 80 m in the deepest section located between the marine infrastructure and Moosehead Island. Deception Bay is accessible from Hudson Strait by boat during the ice-free season, or by icebreaker. It is also accessible in winter and spring by snowmobile from overland trails. The closest communities are Salluit (50 km west) and Kangiqsujuaq (200 km south-east). The study area corresponds to a 9 km long section of the bay, centered on the marine infrastructures (see Fig. 2).

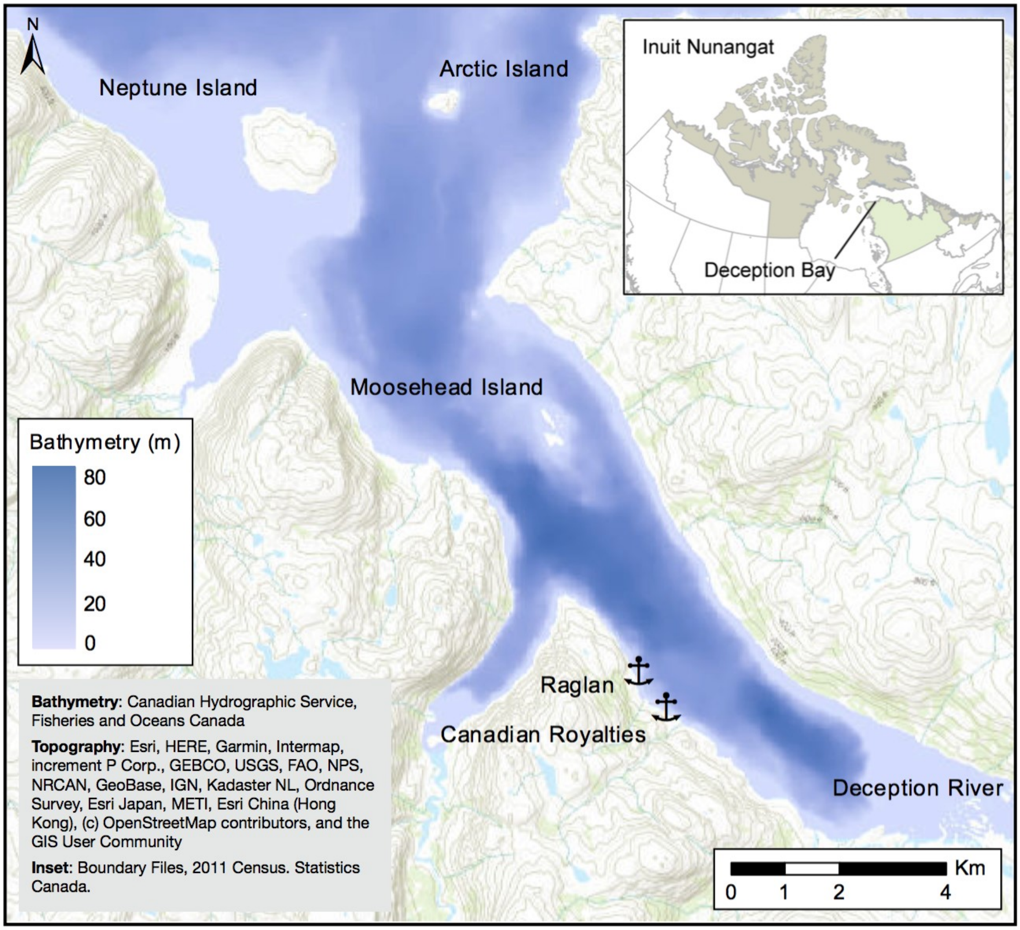

Figure 1: Elevation and bathymetry map of Deception Bay. Inset: Inuit Nunangat, with Nunavik in green. Marine infrastructures are identified with anchor markers.

The Canadian Ice Service, in its *"Climatic Ice Atlas 1981-2010"*, estimates freeze-up and breakup in the bay to occur around the first week of December and the first week of July, respectively (Fequet et al., 2011). Landfast sea ice typically extends to the mouth of the bay, where it is stabilized by Neptune Island. Point thickness measurements performed in Deception Bay for the Ice Monitoring project in January-February and April-May 2016, 2017, and 2018 (Gauthier et al., 2018) ranged from 0 to 55 cm for the snow cover, and 52 to 165 cm for the ice cover. Deception River is the largest river flowing into the bay, and its flow is greatest at the end of spring in June and July because of snowmelt; its flow is almost zero during the winter (GENIVAR, 2012). Water salinity in the bay ranges from 29 to 33 psu (GENIVAR, 2012).

3. Data description

In addition to TerraSAR-X and time-lapse photography data, which is described in this section, air temperature data was also considered. The nearest meterological station is located 50 km west of the study area, at Salluit airport, and partial air temperature measurements are acquired in the bay by time-lapse cameras. These two data sources are presented and compared in the supplementary materials, under “Air temperature in Deception Bay”. Data from Salluit airport is presented in the Results section as either monthly mean air temperature and or monthly cumulative freezing and thawing degree-days (see S9 and S10 in the supplementary materials).

3.1 TerraSAR-X

TerraSAR-X acquired StripMap dual co- and cross-polarization single look complex (SLC) images over Deception Bay from December 2015 to July 2018, spanning three winter seasons. This X-band satellite—and its counterpart TanDEM-X—operate at a central frequency of 9.65 GHz (3.11 cm wavelength), with a repeat period of 11 days. Three orbits overpass the study area (13, 21, 89); orbits 21 and 89 are respectively one and five days later than orbit 13. Each orbit yields a time-series of images with identical acquisition parameters (see Table 1). Their incidence angles range from 38° to 46°, in either ascending or descending passes, and they all include a VV polarization. The scene size before subsetting to the study area was 15 by 50 km, with a spatial resolution of 0.9 and 2.5 m, respectively, for range and azimuth directions (Eineder et al., 2008). Figure 2 shows the extent of the subimages, which cover a 9 km long section of the bay.

Table 1: Characteristics of TerraSAR-X acquisitions for the study.

Orbit	Local acquisition time	Incidence angle	Polarisations	Acquisition period	Total number of images
13	17:32 (ascending)	38°	HH/VV	23 December 2015 to 26 July 2018	75
21	6:25 (descending)	40°	VV/VH	24 December 2015 to 27 July 2018	70
89	17:40 (ascending)	46°	VV/VH	28 December 2015 to 31 July 2018	76

3.2 Time-lapse photography

A pan-tilt-zoom Panasonic WV-SW598 camera was installed on the south-west shore of Deception Bay (Fig. 2) on 11 September 2015. Operating in time-lapse mode, the camera takes a photograph every 15 minutes during the day (from 6:00 to 18:00 local time), rotating through four preset views (Fig. 2). The photographs have an effective pixel count of 2.4 megapixels and a 90x zoom is available when setting the views or taking remote control of the camera. The camera can operate at temperatures between -50°C and 55°C and is installed at a height of 1.8 m. The selected site is accessible by foot from Raglan's marine infrastructure, located on a high-point which offers a good view of the study area. Photographs are automatically transferred through Raglan's network to a database hosted by INRS. There are roughly 1 400 photographs per month, for a total of almost 17 thousand per year, all available to the general public on http://caiman.ete.inrs.ca (Bernier et al., 2017).

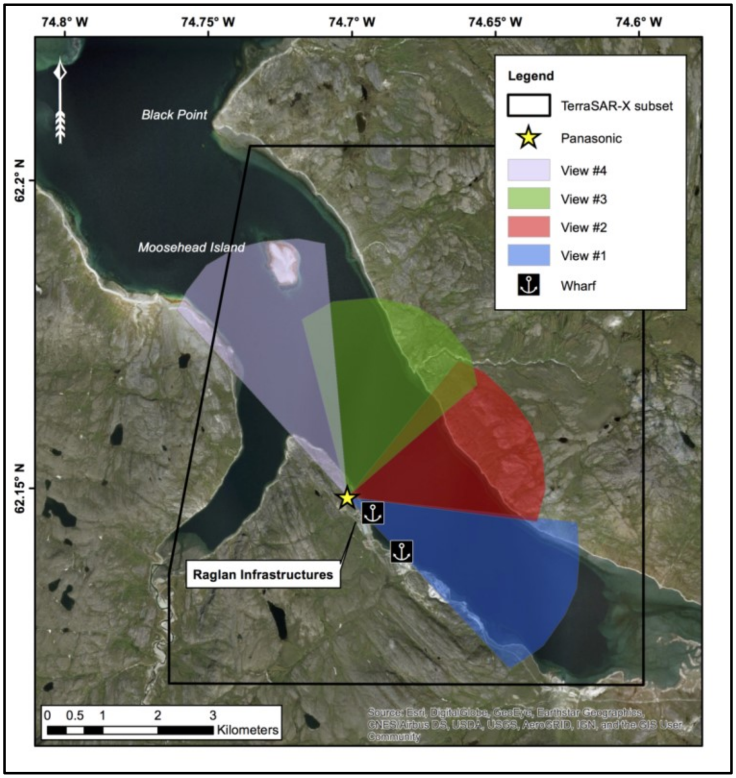

Figure 2: Map of TerraSAR-X image subset, time-lapse camera locations, and Panasonic fields of view.

4. Methods

We chose three general sea ice processes for spatio-temporal monitoring: freeze-up, wintering, and breakup. The wintering process is defined as a general term which may include winter sea ice processes such as ice desalination, snow reorganisation, etc. Specific elements characterizing each process were identified and observed through TerraSAR-X or time-lapse photography indicators. For example, the dates on which freeze-up begins and ends are respectively indicated by the first day where sections of the wintering ice cover are observed on the water and the first day where the wintering ice cover is complete and stable. Sections 4.1 and 4.2 describe the process element indicators and how they are observed or measured from each data source. Section 4.3 details how we compared the photographs with coincident satellite images and identified their features, which serves to evaluate the potential of time-lapse photography to enhance TerraSAR-X image interpretation.

4.1 TerraSAR-X image processing and temporal interpretation

The TerraSAR-X images were used to document both the spatial and temporal aspects of the freeze-up, wintering, and breakup processes. Before being interpreted, the images were first processed at the DLR (German Aerospace Center), using the Multi-SAR System. This workflow starts with a conversion from the digital number to radar brightness (sigma-naught), followed by multi-looking to produce square pixels and increase the radiometric quality (number of looks), orthorectification so all the images from all orbits could be overlaid, and image enhancement to reduce the speckle inherent to SAR images (Schmitt et al., 2015). The Multi-SAR System is described in detail in Bertram et al. (2016). The output images have a geometric resolution of 2.5 m pixels with a radiometric resolution of 1.6 looks. The TerraSAR-X noise floor for the three orbits ranges between -23 and -24.5 dB, and the radiometric accuracy is 0.6 dB (Eineder et al. 2008).

Median backscattering was computed for each subimage and plotted as a function of time for a given year. 32 areas of interest (AOIs) were distributed over the study area, roughly 120 m by 100 m and containing between 2016 and 2064 pixels each. Their locations were chosen to avoid the shore, man-made structures like docks, as well as broken ice left in the wake of ice-breakers (Fig. 3). The median backscattering was computed over each AOI, and then over all AOIs for a given subimage, yielding a single median value per subimage. This step was performed using Python (Dufour-Beauséjour, 2019).

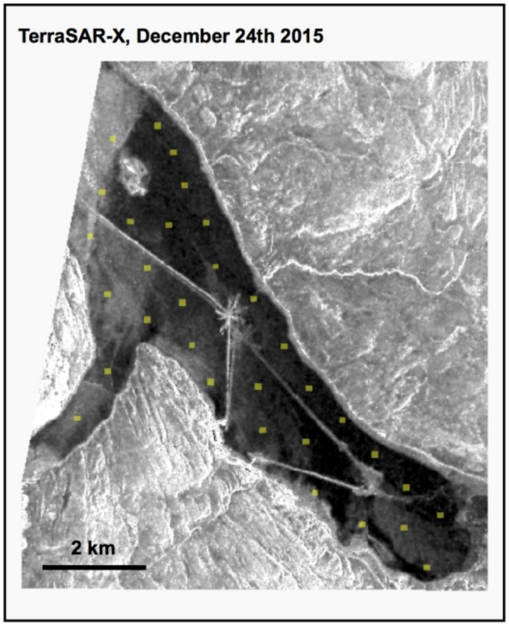

Figure 3: TerraSAR-X VV subimage of Deception Bay on 24 December 2015 in orbit 21 and AOIs used to compute statistics (yellow). The image is grey-scaled from -19 to -5 dB.

Recurring seasonal features in all X-band VV median backscattering time-series acquired during this study include two peaks separated by a monotone period. From this, four indicators were derived: the post-freeze-up peak (I), the beginning (II) and end (III) of the monotone period, and the spring peak (IV). Figure 4 shows examples for two different years and orbits, chosen for their clarity. Speaking in terms of the data time-series, peak location is defined as the location of its maximum and estimated as sitting between the left and right-hand neighbors of the highest data point. The beginning (end) of the monotone period is estimated as sitting between the first (last) monotone data point and its left-hand (right-hand) neighbor. Figure 4 shows an example of estimated ranges for each indicator, using two orbits and years chosen for their clarity. These ranges were identified manually and are presented for all orbits and years in the supplementary materials (Fig. S1-S3). The estimated range for a given indicator and year was further reduced by combining all available orbits (Fig. S1-S3). Finally, the winter trend was computed from a linear regression fit on the data in the monotone period, as shown in the supplementary materials (Fig. S4).

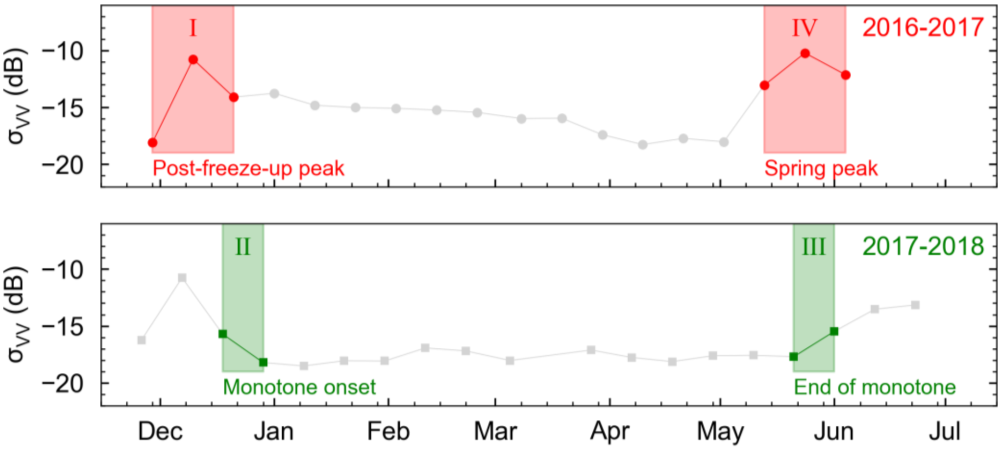

Figure 4: Examples of change detection in TerraSAR-X VV median backscattering. Peak detection for orbit 21 in 2016-2017 (top), and inflexion detection for orbit 13 in 2017-2018 (bottom).

4.2 Photograph interpretation

The photographs were interpreted to document both the temporal and spatial aspects of freeze-up and breakup processes. The freeze-up process includes the formation of various ice types in the study area up to their eventual consolidation into a continuous ice cover which stays in place for the whole winter. The breakup process includes the degradation and dislocation of the ice cover up to the total absence of ice.

During the freeze-up process, ice types were identified following WMO nomenclature as either grease ice (a soupy and matt layer of coagulated crystals), shuga (an accumulation of spongy white lumps a few centimeters accross), nilas (a thin crust of matt ice which may raft in interlocking fingers), ice rind (a brittle and shiny crust of ice formed on a quiet surface, easily breaking into pieces), and pancake ice (pieces of ice up to 3 meters in diameter which may be formed from the preceding types of ice and rapidly cover large expanses) (descriptions from WMO, 2014).

Consolidation of the ice cover was documented based on the persistence of features over time and their lateral movement. The date on which the freeze-up process was completed, called “the freeze-up date”, was also used as an indicator. For the breakup process, ice cover dislocation was documented based on the occurrence of open water. Ice cover degradation was documented based on its color and texture, as well as the occurrence of flooding. The date on which the breakup process was completed, called “the breakup date”, was also used as an indicator. Photograph sequences showing the freeze-up and breakup processes for each season are presented in the supplementary (Movies S1-S6).

Figure 5 shows two examples of photograph interpretation. At the top, the 2016 breakup process unfolds: snow and ice covers degradation can be seen through changes in color and texture. At the bottom, the 2016 freeze-up process comes to an end on 29 November, where nilas patches on the water consolidate into a continuous ice cover whose features are immobile.

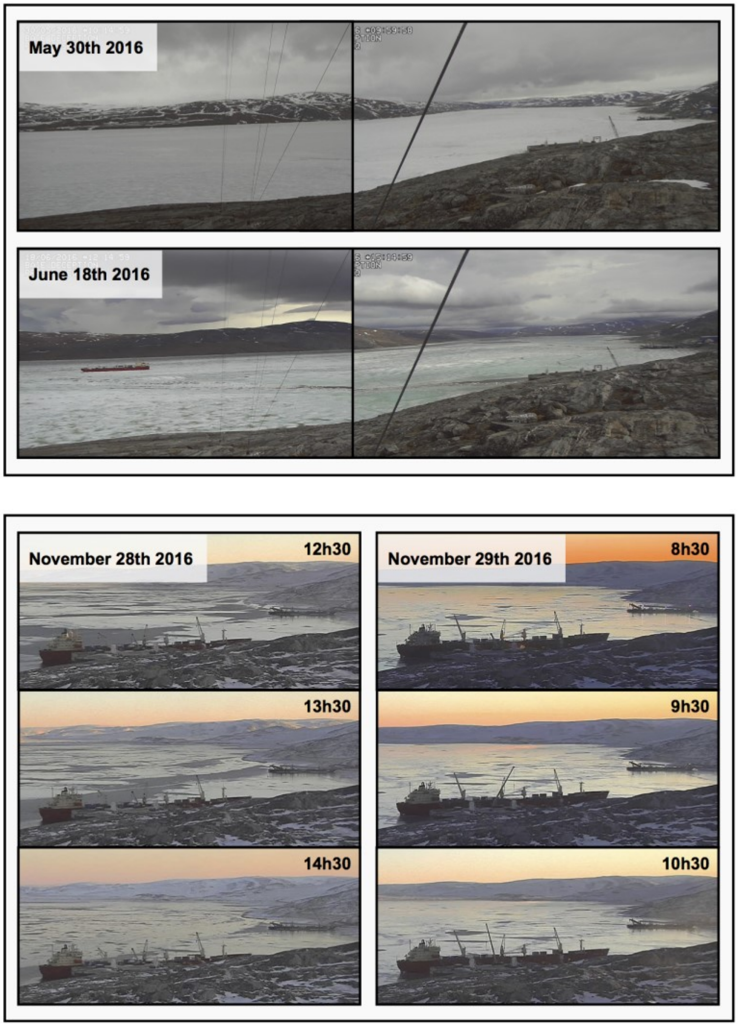

Figure 5: Time-lapse photography during the 2016 breakup process (top) and the 2016 freeze-up process (bottom).

4.3 TerraSAR-X spatial interpretation using photography

TerraSAR-X images were interpreted using coincident photographs taken from the shore. Observed features include open water areas or leads and different ice types. Figure 6 shows two examples. At the top, nilas, pancake ice and grease ice are observed on the photographs during the 2017 freeze-up process, and then identified on a coincident TerraSAR-X image acquired on 26 November. At the bottom, ice cover dislocation is observed on photographs during the 2018 break-up process; leads and open areas are identified on the coincident 28 June image.

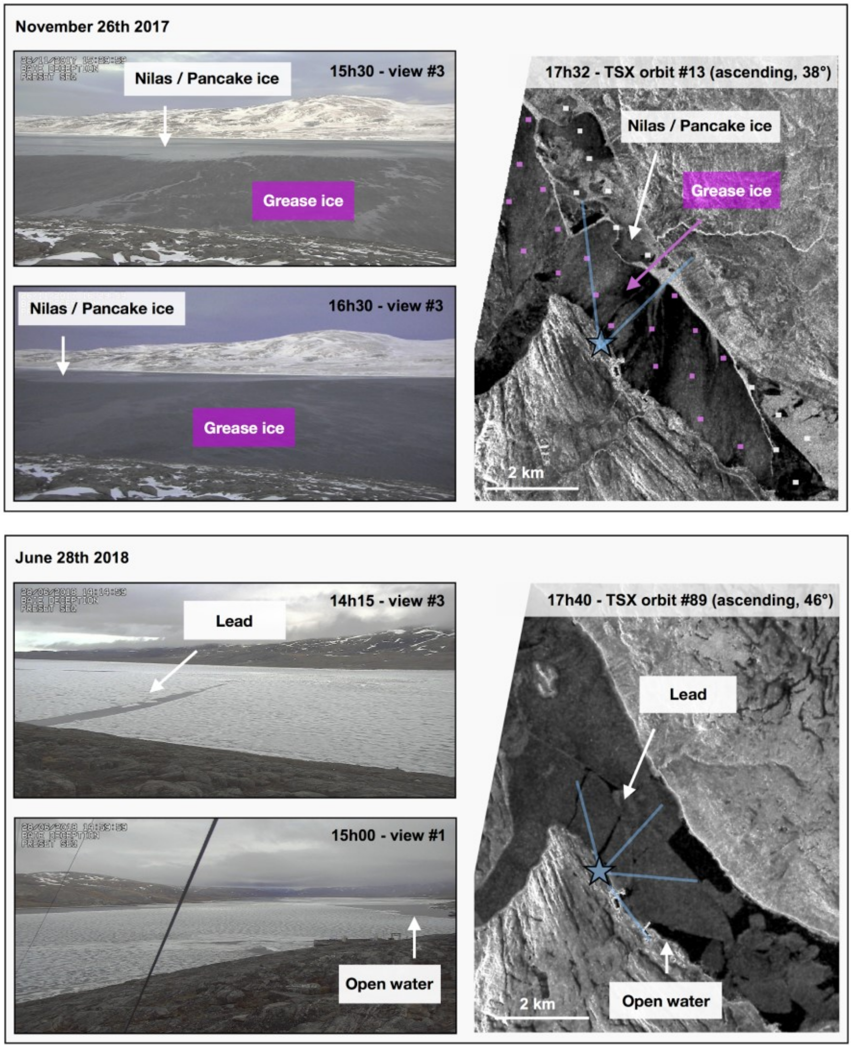

Figure 6: Coincident time-lapse photography and TerraSAR-X images during the 2017 freeze-up process (top) and the 2018 breakup process (bottom). On the images, camera location and fields of view are identified in blue. Top: TerraSAR-X VV image from orbit 13. AOIs are color-coded according to the identified ice type, prior to backscattering signature extraction. Bottom: TerraSAR-X VV image from orbit 89. Both images are grey-scaled from -19 to -5 dB.

5. Results

Results from the methods described above are spatio-temporal descriptions of sea ice seasonal processes, organized here following the seasons (freeze-up, wintering, and spring). Results from different sources and methods are presented together to facilitate interpretation.

5.1 Freeze-up

In the following description of processes for each year, we refer to zones represented in Fig. 7. No ice-breaker transits occurred during the freeze-up process for the three years of this study. The freeze-up date is the first day featuring a consolidated ice cover which remains in place for the whole winter.

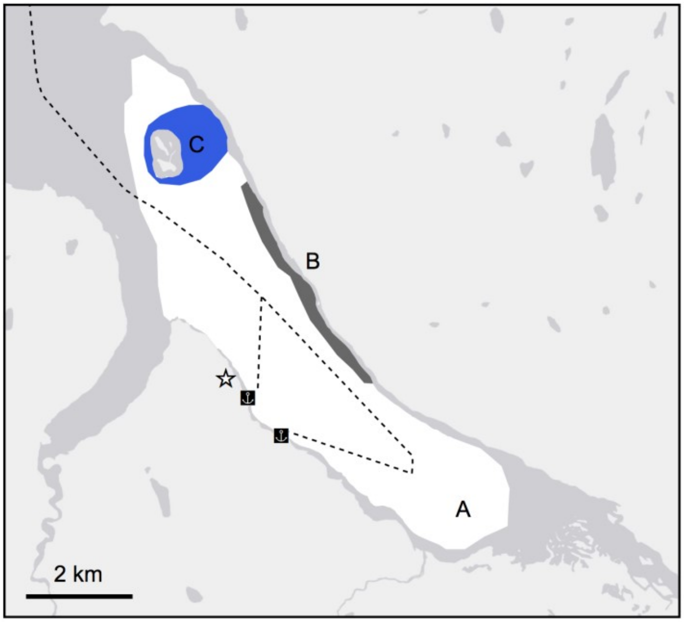

Figure 7: Zones relevant for describing the spatial aspects of the freeze-up process in Deception Bay, and ship routes for the MV *Arctic* and MV *Nunavik* (dashed line). Camera location is indicated with a star.

In 2015, freeze-up was preceded by days featuring fog and open water, as well as grease ice and shuga. On 10 November, landfast ice appeared along the north-eastern shore (zone B) and grew thermally, progressively extending to cover the whole study area (zone A) by 11 November 2015. In 2016, the days before freeze-up featured grease ice and open water, and the accumulation of pancake ice over the shallows near Moosehead Island (zone C). After the formation of nilas and various new ice types on 27 November, zone A was covered by mirror-like patches of nilas and ice rind on 28 November. Their lateral movement is illustrated in Fig. 5. The next morning, overlapping patches of nilas covered the study area. No lateral movement of the ice was observed on 29 November. Freeze-up was therefore completed on 29 November 2016. In 2017, a similar series of events was observed. Freeze-up was alternatively preceded by days of open water and days where the water was covered in grease ice or nilas, and pancake ice accumulated in zone C. On 27 November, zone A was covered with mirror-like nilas or ice rind. This ice was rearranged during the night into an ice cover which showed no further substantial lateral movement.

Observed features shifted slightly south-east in the night between 29 and 30 November. Despite these minor tidal movements, we identify freeze-up as having occurred on 28 November 2017.

Following ice type identification from photographs, the X-band backscattering signature of newly formed ice types was extracted during the 2016 and 2017 freeze-up processes. An example of TerraSAR-X image interpretation from coincident photographs is shown in Fig. 6, where grease ice was observed as well as a mix of nilas and pancake ice. Figure 8 shows median VV backscattering values for AOIs over grease ice, nilas, pancake ice, and a mixture of the two. In the days following the 2016 and 2017 freeze-up dates, the young ice cover presented systematically higher backscattering than during the rest of the winter. Identification of a specific ice type was impossible from time-lapse photography however, since young ice is characterized by its thickness (WMO, 2014). Figure 8 also shows median VV backscattering for AOIs over this unidentified young ice. Results are presented for different acquisition geometries and incidence angles (details in figure caption). The images associated with each box in Fig. 8 are reproduced in the supplementary materials (Fig. S5-S6) along with the color-coded AOIs used for each ice type.

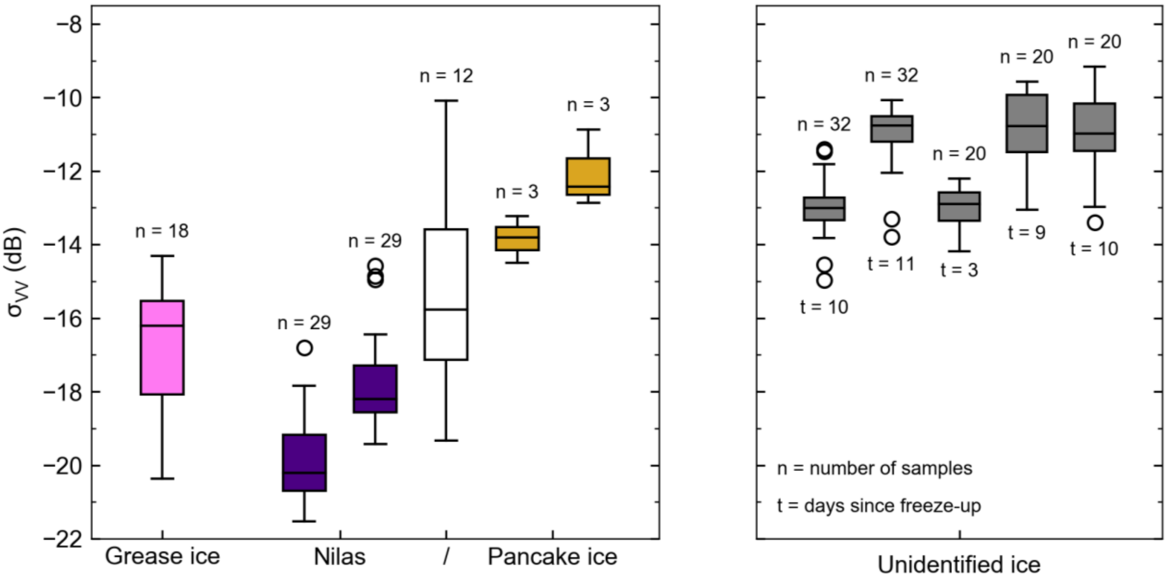

Figure 8: TerraSAR-X median VV backscattering values observed over AOIs of ice types identified from time-lapse photography in 2016 and 2017. The number of median values used (n) is written above each box. Outliers are plotted as empty white circles. Left: Grease ice (pink) was observed on the orbit 13 image from 26 November 2017. Nilas (dark purple) was observed on 28 and 29 November 2016 in orbits 13 and 21, respectively. A mix of nilas and pancake ice (white) was observed on 26 November 2017 in orbit 13. Pancake ice (yellow) was observed on 28 and 29 November 2016 in orbits 13 and 21. Right: Unidentified young ice (grey) was observed on 9 and 10 December 2016 in orbits 13 and 21, as well as on 1, 7 and 8 December 2017 in orbits 89, 13, and 21. The number of days since the freeze-up date (t) is written below each box.

Figure 9 shows the temporal evolution of the median VV backscattering during the freeze-up processes, as well as indicators derived from time-lapse photography and TerraSAR-X: the freeze-up date, the freeze-up peak (I), and the beginning of monotone backscattering (II). No TerraSAR-X data is available during freeze-up 2015. The daily event sequence (Tables S1-S3), as well as videos assembled from time-lapse photography (Movies S1-S3) and TerraSAR-X (Movies S7-S9), are available as supplementary materials. 2015 saw an earlier freeze-up than the other years by 18 and 17 days (2017 and 2018). Mean temperatures measured over the years at Salluit airport for October ranged from -3°C in 2017 to -5°C in 2015, and from -8°C in 2016 to -11°C in 2015 for November (see Fig. S9 in the supplementary materials).

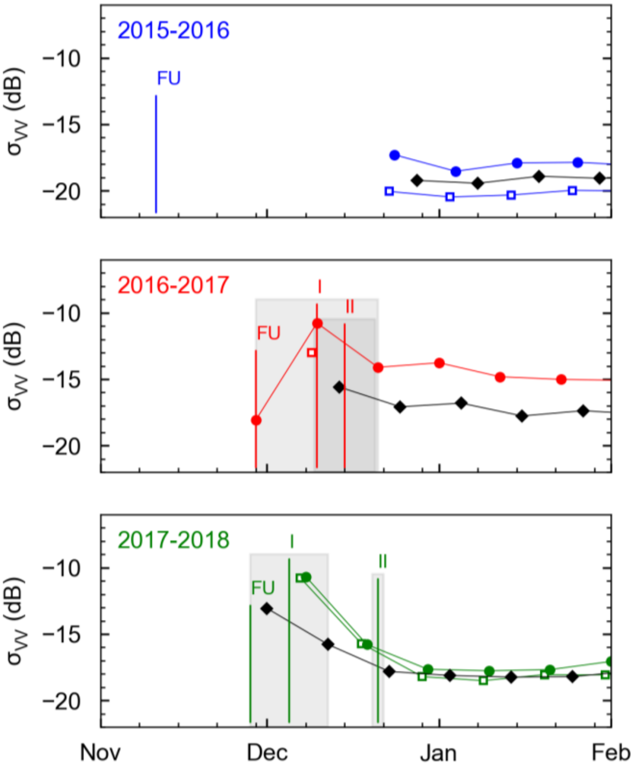

Figure 9: TerraSAR-X median VV backscattering is plotted versus time for each year (color-coded). Three orbits are shown for: orbits 13 (empty square), 21 (circle), and 89 (black diamond). The freeze-up date (FU, from time-lapse photography), the post-freeze-up peak (I, from TerraSAR-X), and the beginning of monotone X-band (II, from TerraSAR-X) are identified with vertical bars. Estimates for each indicator are indicated by shaded grey areas.

5.2 Wintering

The coldest months were observed in 2017-2018, with mean January and February temperatures measured at Salluit airport sitting at -27 and -30°C, respectively (see Fig. S9 in the supplementary materials). For the purpose of characterizing the winter backscattering signature of snow-covered sea ice, winter is defined from the TerraSAR-X time-series as the monotone period between the post-freeze-up peak and the spring peak. Derivation of these limits is presented in the supplementary materials (Fig. S3).

Figure 10 shows the X-band winter backscattering signature of snow-covered sea ice in Deception Bay, or “white ice” in WMO terminology. Median backscattering observed for white ice ranged from -14 to -20 dB over the three years. In winter 2015-2016, the median was consistently lower than for the other two years, across orbits. Winter values were systematically higher for the descending/morning orbit than for the ascending/evening ones. In 2016-2017, all orbits show a negative winter trend (Fig. 10). This trend is most pronounced in the descending/morning data, which also shows a larger spread than in the other orbits (Fig. 10). Meanwhile, the 2015-2016 and 2017-2018 backscattering time-series exhibit little to no winter trend.

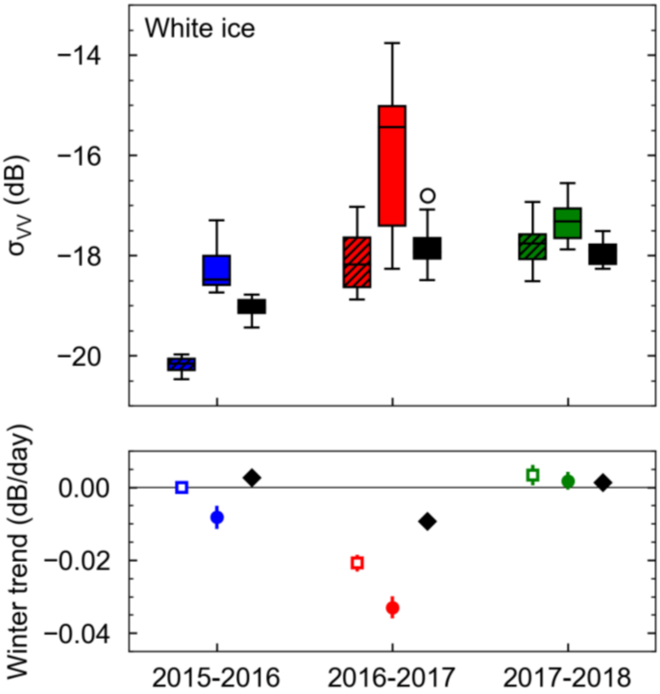

Figure 10: Characterization of TerraSAR-X VV winter backscattering. Top: Winter median by year (color-coded) for orbits 13 (dashed, ascending, 5:32 PM, 38°), 21 (solid, descending, 6:25 AM, 40°), and 89 (black, ascending, 5:40 PM, 46°). The seasonal median is computed from image medians, which were computed from AOI medians. Empty circle markers represent outliers. Bottom: Winter trend by year (color-coded), for orbits 13 (empty square), 21 (circle), and 89 (black diamond). A horizontal black line indicates the point of zero trend. The trend is defined as the slope of the linear fit to the winter image medians (see Fig. S6). Error bars are the standard error associated with the fit.

5.3 Spring

In the following description of each year's breakup, we refer to zones represented in Fig. 11. The breakup date is the first day when the study area is ice-free.

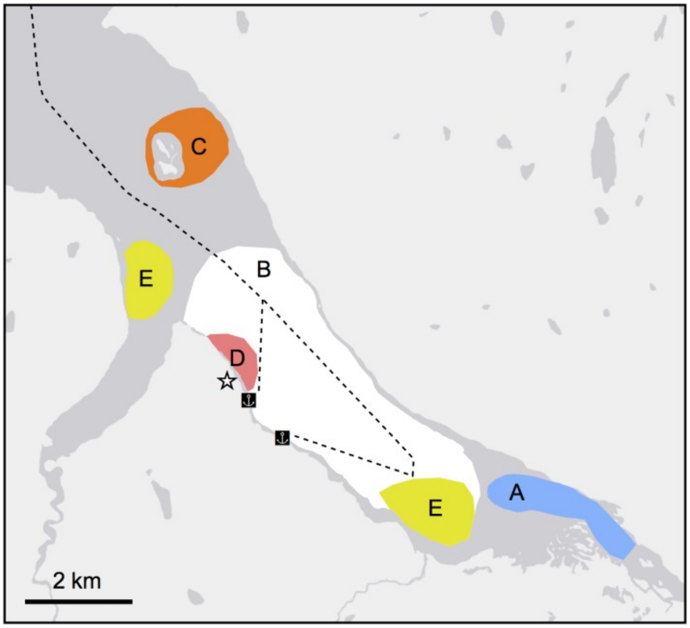

Figure 11: Zones relevant for describing the spatial aspects of breakup in Deception Bay and ship routes for the MV *Arctic* and MV *Nunavik* (dashed line). Camera location is indicated with a star.

In 2016, patches of bare ice could be observed throughout the winter, particularly along the south-west shore (zone D). This bare ice started to appear rougher on 20 May. Despite ice-breaking manoeuvers performed by the MV *Nunavik* in zone B upon its arrival in the bay on 16 June, no open water could be seen along its tracks either on the photographs or on the TerraSAR-X image from the same day. Deception River thawed by 16 June. Zone D was seen to be covered in meltwater on 18 June, and open water was first observed on 19 June, in front of the river (zone A). Open water progressed steadily throughout zone B over the course of five days, until Moosehead Island (zone C) was also ice-free and breakup was completed on 24 June 2016.

In 2017, snow rapidly melted off following the end of the monotone backscattering period. By 13 May, more than two thirds of zone B was snow-free, before a snowfall event on the 14 May. On 31 May, the ice featured meltwater ponds. Deception River had thawed by 3 June (zone A), and on 4 June some open water could be seen along the ship tracks near zone D. Breakup took eight days and followed the same spatial pattern as the year before. Breakup was completed with the freeing of zone C on 12 June 2017. In 2018, the snow cover appeared largely melted on the south-eastern part of zone B by 28 May, and meltwater was seen on the ice on several occasions mid-June (zones E). The MV *Nunavik* and MV *Arctic* entered the bay on 17 June. Six days later, open water could be seen along most of the ship tracks and the river had thawed. The ships' departure coincided with the first day where meltwater ponds covered the ice. New cracks perpendicular to the shore appeared in the ice that day. These features can be seen on photographs (Fig. 6). Open water was first observed near the south-east shore in zone B on 26

June. The TerraSAR-X image acquired that day (Fig. 6) shows large ice pieces separated along the ship tracks and floating freely in zone B. The breakup was completed on 3 July 2018, seven days after the first observation of open water.

Figure 12 shows the temporal evolution of the median VV backscattering during the breakup process, as well as indicators derived from time-lapse photography and TerraSAR-X: the end of monotone backscattering (III), the spring peak (IV), and the breakup date. The daily event sequence (Tables S4-S6)—including ice-breaker transits—as well as videos assembled from time-lapse photography (Movies S3-S6) and TerraSAR-X (Movies S7-S9), are available as supplementary materials. 2016 saw both the earliest end of monotone backscattering and the longest period between this and breakup—59 days compared to 35 both in 2017 and 2018. May 2017 stands out with 57 thawing degree-days compared to 4 and 0 in May 2016 and 2018 respectively (see Fig. S10 in the supplementary materials).

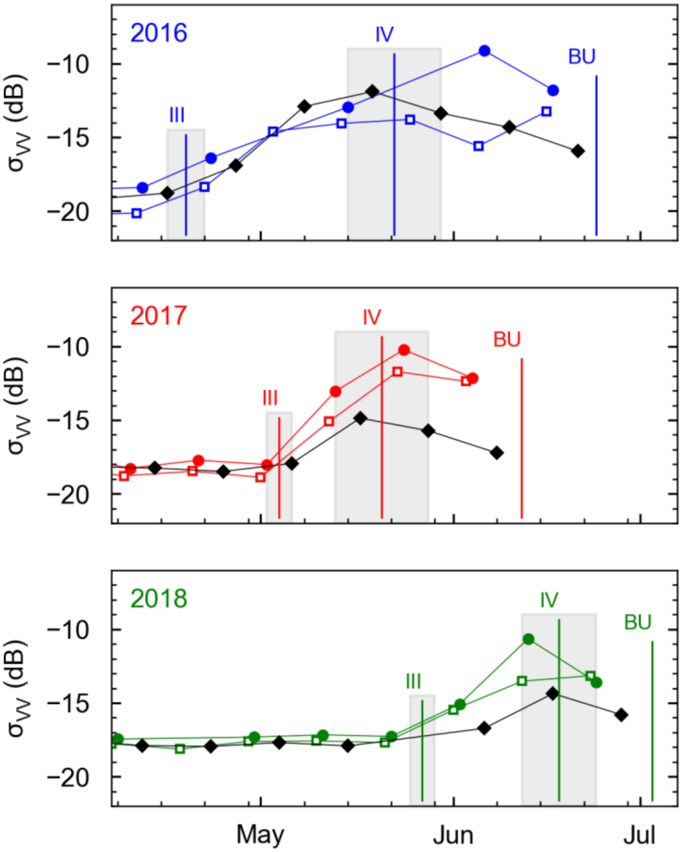

Figure 12: TerraSAR-X median VV backscattering is plotted versus time for each year (color-coded). Three orbits are shown: orbits 13 (empty square), 21 (circle), and 89 (black diamond). The end of monotone X-band (III, from TerraSAR-X), spring peak (IV, from TerraSAR-X), and the breakup date (BU, from time-lapse photography), are identified with vertical bars. Estimates for each indicator are indicated by shaded grey areas.

6. Discussion

The use of TerraSAR-X and time-lapse photography time-series for seasonal monitoring of sea ice processes is first discussed for each data source as a stand-alone monitoring tool (Sect. 6.1), and then for their combination (Sect. 6.2). Processes observed in Deception Bay using these tools (freeze-up, wintering, melting and ponding, and breakup) are then discussed in Sect. 6.3.

6.1 Data sources as stand-alone monitoring tools

6.1.1 TerraSAR-X

With a revisit period of 11 days, each TerraSAR-X time-series provided access to the seasonal scale of processes. For example, spring features consistently present in all nine datasets for this study (Fig. 12) were associated with springtime melt/thaw processes, as discussed in Sect. 6.3.3. Faster processes could not be resolved, such as freeze-up which unfolded over one to three days (see Sect. 5.1). Spatially, TerraSAR-X offered the advantage of uniform coverage for the whole study area. This allowed us to document the 2018 breakup spatial pattern (Fig. 6). Success on this front is however dependent on lucky timing. Interpretation of the spectral aspect of sea ice processes was hindered by the relative lack of literature specific to X-band backscattering. Indeed, despite their spectral proximity, the C-band and X-band have been shown to behave differently when it comes to interaction with brine-wetted snow for instance (Nandan et al., 2016). A study of X-band scattering mechanisms and the associated physiochemical properties of snow and sea ice, although needed, is outside the scope of this paper.

6.1.2 Time-lapse photography

Hourly photographs allowed for the detailed observation of daily or weekly processes, for instance freeze-up. Observations were limited by the absence of photographs during the night and by low visibility periods caused by fog or blowing snow. Spatially, interpretation was limited to the camera's field of view. Details too small (e.g. frost flowers) or too far away (melting of Deception River) could not be resolved. Distances were hard to evaluate on the photographs, which limited the interpretation of feature size or of their extent on the bay (e.g. melt ponds). As for the spectral manifestation of processes, interpretation was straightforward because the photographs were in the visible spectrum. This also allowed for the observation of some meteorological conditions like snowfall (see Tables S1-S6).

6.2 Complementarity of the data sources

The combination of TerraSAR-X and time-lapse photography allowed us to use the strengths of one data source to mitigate weaknesses from another. For example, the TerraSAR-X images acquired during the break-up processes filled in some gaps regarding the state of Deception River (frozen or thawed), which was too far to be resolved on the photographs. Conversely, photography allowed us to compile a daily event sequence of breakup-related events (Tables S3-S6). Overlap of the data sources (e.g. Fig. 6) allowed for co-interpretation, which was used to document the X-band backscattering signature of several newly formed ice types (see Fig. 8), as discussed in Sect. 6.3.1.

6.3 Sea ice processes observed in Deception Bay

6.3.1 Freeze-up

Two different freeze-up processes were documented over the course of the study, as presented in Sect. 5.1. In 2015, calm waters allowed for a quick thermal freeze-up. Below-zero temperatures were earliest in 2015, with the coldest months of October, November, and December of the three years (see Fig. S3-3). In 2016 and 2017, freeze-up rather proceeded iteratively, from patches of nilas and ice rind. We speculate that the first process produced smoother ice than the second process. For a given incidence angle, winter backscattering was systematically lower in 2015-2016 than in the other two years (Fig. 10), which we attribute to a smaller surface scattering component that year.

We presented values of -16 ± 2 dB for grease ice and -19 ± 2 dB for nilas in VV at 38° to 46° (Fig. 8), which is higher than the -22.0 ± 0.5 dB value reported by Nakamura et al. (2005) for new ice (defined as including frazil, grease ice, and nilas), observed in the same polarization and similar incidence angles of 39° to 44°. Our values are also higher than the -21 dB value reported by Matsuoka et al. (2001) for snow-free thin ice (defined as including nilas and grey ice) observed in HH at lower incidence angles of 22° to 25°. The backscattering signature of grease ice, which may form waves in the presence of wind, may depend on environmental conditions (Isleifson et al., 2010), which limits comparison. Several factors may be intervening in backscattering from nilas. In cold and dry snow conditions, the X-band is not expected to penetrate significantly in the ice cover, with backscattering dominated by the presence of brine at the snow-ice interface (Nandan et al., 2016). Frost flowers are known to increase the backscattering from newly formed sea ice in the C-band, an effect which may be more pronounced over thin ice; an increase of 5 dB was reported over ice 2 to 15 cm thick (Nghiem et al., 1997), and of 13 dB over 5 cm thick ice (Isleifson et al., 2014). Snow may also lead to an increase in backscattering through warming of the snow-ice interface and an associated increase in brine scatterer size (Gill et al., 2015). In the case of our nilas observations, snow itself might be enough to explain the 3 dB difference; frost flowers may also have played a role, but could not be observed on the photographs.

Despite a difference of almost 20° in the incidence angle, our observation of -12 ± 1 dB over unidentified ice one to nine days after freeze-up (Fig. 8) is close to reports by Johansson et al. (2017) of -11.9 dB over new ice (defined as including nilas, grey ice, and white ice up to 50 cm thick) observed in the X-band VV at 25°, as well as to reports by Onstott (1992) of -14.4 dB over thin first year ice (30 to 70 cm thick) in the X-band HH at 23°. The post-freeze-up peak and monotone backscattering onset are also observed in C-band time-series over sea ice (Yackel et al., 2007), but these seasonal features have been less studied than their spring counterparts (end of monotone backscattering and spring peak). Moreover, similar features observed in X and C-band time-series could well be related to different scattering mechanisms, and even to different physical processes. We limit ourselves to speculating, for the X-band data presented in this manuscript, that the increasing portion of the backscattering peak may be associated with the domination of surface scattering related to a brine-rich ice surface, potentially covered in frost flower, and that the decreasing portion may be associated with a transition to an absorption regime, in which the signal suffers loss in the brine-wetted and increasingly colder snow.

6.3.2 Wintering

Although specific winter sea ice processes exist, for instance sea ice desalination, snow accumulation and reorganization, time-lapse photography did not allow us to document them. TerraSAR-X time-series may however have potential for such monitoring, although another source of data is needed to support interpretation. In general, our backscattering time-series fall within the -10 and -20 dB range reported by Onstott (1992) for first-year ice observed with X-band HH or VV at 40° between January and June.

Before moving on to the spring processes, we first discuss the influence of an 8° difference between ascending orbits 13 and 89. For 2016-2017 and 2017-2018, a small incidence angle effect was seen during the post-freeze-up and spring peaks, where backscattering was 1 to 3 dB smaller at the higher incidence angle (see Fig. 9 and 12), while none was seen during the monotone winter period (see Fig. 10). A backscattering signal which decreases with incidence angle is expected for situations dominated by surface scattering on a relatively rough surface (Ulaby et al., 1986). In the C-band, surface scattering at the interfaces between dry snow, brine-wetted snow, and ice is indeed expected to dominate for cold snow-covered sea ice, with a transition to mixed scattering for thicker snow covers (Gill et al., 2015). We speculate that surface scattering explains the small incidence angle effect observed in our X-band data. 2015-2016 however presents a very different case. Backscattering at the higher incidence angle is consistently 2 dB higher than at the lower incidence angle, throughout winter and during the spring peak (see Fig. 12). The freeze-up process was different that year compared to 2016 and 2017 and we have already suggested that the ice cover was much smoother for the 2015-2016 season. We speculate that surface scattering was comparatively low that year, and that volume scattering, which Ulaby et al. (1986) have shown can slightly increase with incidence angle, dominated instead.

An acquisition time effect can be seen in the winter data (Fig. 10): the descending/morning winter median was systematically higher than in either ascending/evening orbits. Temperatures in the snow and ice covers are expected to be higher following daytime than in the morning. Dielectric loss in the C-band is known to increase with temperature for snow on sea ice (Gill et al. 2015). We speculate that backscattering might be lower in general in the evening than in the morning due to increased dispersion in the warmer medium.

6.3.3 Melting and ponding

Monotone X-band backscattering was observed every winter of the study, for all incidence angles and acquisition times, before a systematic springtime increase in backscattering. In the C-band, winter is also characterized by monotone backscattering, ending with melt onset brought on by warmer air temperatures (Yackel et al., 2007). Mechanisms which may increase C-band backscattering from snow-covered sea ice include surface scattering from the brine-wetted layer at the bottom of the snowpack (Nandan et al., 2016), volume scattering on brine inclusions enlarged by an increase in temperature (Barber and Nghiem, 1999), and surface scattering on wet snow (Gill et al., 2015; Yackel et al., 2007) accumulated at the top of the snowpack due to above-zero temperatures and solar radiation (Gogineni et al., 1992; Kim et al., 1984). We speculate that the X-band is susceptible to all of these C-band mechanisms, with an emphasis on surface scattering due to its lower penetration depth (Nandan et al., 2016), and attribute the end of X-band monotone backscattering to melt onset.

Springtime backscattering was seen to eventually peak in all TerraSAR-X datasets (Fig. 12), although one series featured more than one maximum (orbit 13, 2015-2016), another none (orbit 13, 2017-2018), and an apparent mismatch between maximum location in the 2015-2016 data. In the C-band, springtime peaking of the backscattering is attributed to the transition from the pendular regime (Yackel et al., 2007; Barber et al., 1995), where water is held in the snowpack (Scharien et al., 2012) and backscattering increases as described in the last paragraph, to the funicular regime where meltwater drains downward (Scharien et al., 2012), flushing out brine (Barber et al., 1995), and potentially refreezing (Gogineni et al., 1992). The decrease in C-band backscattering, which forces its peaking, is attributed to a decrease in the dielectric constant of the snowpack following the transition to the funicular regime (Yackel et al., 2007). We speculate that the decrease in the X-band springtime backscattering is also caused by pond onset, and associated with increased penetration in the drained snowpack.

Neither melt or pond onset could be resolved using time-lapse photography, although signs of ice cover degradation were eventually observed and used to document break-up (see example in Fig. 5). Table 2 shows melt and pond onset timing estimated by combining the three TerraSAR-X time-series. 2016 showed the earliest melt onset, and the longest period separating it from pond onset (33 days). 2017 showed the shortest time separating melt onset from pond onset (16 days), and the earliest pond onset of the three years. 2018 showed the latest melt and pond onsets, separated by 22 days. This is consistent with air temperature data from Salluit airport; 2018 had the coldest months of May and June (see Fig. S3-3). Meltwater was observed on the ice surface 27 and 11 days after pond onset in 2016 and 2017 respectively, and the day before in 2018, as shown in the supplementary (Tables S4-S6).

6.3.4 Break-up

Two different breakup processes were observed over the course of the study, as presented in Sect. 5.3. In 2016 and 2017, open water was first observed near Deception River and its extent progressed towards the rest of the bay until the whole study area was ice-free. This contrasts with 2018 where, although open water was also first observed near Deception River, breakup was rather characterized by the presence of large ice floes which floated in the bay for a week before disappearing overnight, signalling breakup completion. In 2016, breakup began three days after the *MV Nunavik* first entered the bay in the spring. The first ice-breaking transit of the season occured respectively three days before and one day after the beginning of breakup 2016 and 2017. The 2016 breakup started 28 days after pond onset, compared to the 16 days period observed in 2017. We speculate that the ice cover was in a more advanced state of degradation when breakup started in 2016 than in 2017. This is supported by time-lapse photography which show that the ice cover was partly mobile (under the effect of wind or current) during breakup 2016, but mostly landfast during breakup 2017 (Movies S4-S5). In 2018's comparatively late spring, both the *MV Nunavik* and *MV Arctic* entered the bay during pond onset (on June 17th). Open water was observed along their tracks in the following days and new cracks perpendicular to the shore appeared when the ships left the bay eight days later. In 2016 and 2017, the last area to be cleared of ice was Moosehead Island and its shallows.

With the data available, it is hard to evaluate the impact of shipping on the breakup process in Deception Bay, be it on its pattern, timing, or length. What we can say is that 1) the breakup spatial pattern followed shipping tracks in 2018, but did not in 2016 and 2017; 2) breakup lasted 5, 7, and 7 days in 2016, 2017, and 2018, respectively, and 3) it was completed respectively 33, 23, and 15 days after pond onset. Future work on this front would do well to consider the melting of the ice from underneath due to currents, an important aspect of breakup (Laidler and Ikummaq, 2008) which is hard to access using TerraSAR-X and time-lapse photography.

6.3.5 Seasonal timeline and caveats

Table 2 presents a timeline for the elements relating to sea ice processes which were studied using TerraSAR-X and time-lapse photography indicators. Two indicators derived from backscattering time-series could not be associated with specific elements of sea ice processes: these are the post-freeze-up peak and the beginning of monotone X-band.

Table 2: Seasonal timeline for snow-covered sea ice for three years. Process elements derived from time-lapse photography (Photo.), and TerraSAR-X (TSX) indicators.

Indicator Process element	2015-2016	2016-2017	2017-2018	Photo.	TSX
First day where sections of the wintering ice cover are observed on the water:					
Beginning of freeze-up	Nov. 10th	Nov. 27th	Nov. 26th	x	
First day where the wintering ice cover is complete and stable:					
Freeze-up	Nov. 11th	Nov. 29th	Nov. 28th	x	
Day where, following freeze-up, backscattering is at its highest:					
Unidentified	-	Dec. 10th	Dec. 5th		x
Day where, following the post-freeze-up peak, backscattering becomes monotonous:					
Unidentified	-	Dec. 15th	Dec. 21st		x
Day where the backscattering stops being monotonous after winter:					
Melt onset	Apr. 19th	May 4th	May 27th		x
Day where, following winter, backscattering is at its highest					
Pond onset	May 22nd	May 20th	Jun. 18th		x
First day where open water is observed in place of a previously undisturbed winter ice cover:					
Beginning of breakup	Jun. 19th	Jun. 5th	Jun. 26th	x	
First day where the water is completely ice-free:					
Breakup	Jun. 24th	Jun. 12th	Jul. 3rd	x	

This seasonal timeline relies on the assumptions that 1) freeze-up, wintering, and breakup processes occur each year, that 2) despite interannual differences in timing and spatial extent, the process elements listed in Table 2 always occur, and that 3) the TerraSAR-X and time-lapse photography time-series indicators are always a manifestation of these process elements. This may not always be the case; for instance, melting and ponding is known to be hard to resolve in the C-band for thin ice covers (Yackel et al., 2007), and two of the X-band-derived indicators could not be reliably associated to process elements.

7. Conclusion

This article presented a case study for the seasonal monitoring of sea ice processes using a combination of TerraSAR-X and time-lapse photography time-series. The two data sources proved complementary, their combination enabling spatio-temporal coverage of the processes. It also led to the reporting of new X-band backscattering values over newly formed sea ice types. TerraSAR-X time-series showed potential for tracking melt and pond onset. Finally, we documented two types of freeze-up and breakup processes for Nunavik's Deception Bay, an area at the confluence of climate change, land use by local Inuit, and ice-breaking transport by the mining industry. These processes were seen to depend on geomorphological features such as Moosehead Island and Deception River. Future work in the Ice Monitoring project will build on this characterization of seasonal processes and focus on spatial variations within the bay and comparison with similar fjords, namely Salluit and Kangiqsujuaq. It will also involve comparison of the TerraSAR-X time-series data with RADARSAT-2 time-series acquired over the same period and area.

Code and data availability: The complete time-lapse photography database can be accessed at http://caiman.ete.inrs.ca (Bernier et al., 2017). Quicklooks for the TerraSAR-X images are available on https://doi.pangaea.de/10.1594/PANGAEA.905246 (Dufour-Beauséjour et al. 2019). The code used to compute pixel statistics from the TerraSAR-X images on areas of interest is available at https://github.com/sdufourbeausejour/tiffstats (Dufour-Beauséjour, 2019).

Video supplement: Movies S1, S2, and S3 respectively show the freeze-up sequence for 2015, 2016, and 2017. Movies S4, S5, and S6 respectively show the breakup sequence for 2016, 2017, and 2018. They are available online at https://doi.pangaea.de/10.1594/PANGAEA.904956 (Dufour-Beauséjour et al. 2019). Movies S7, S8, and S9 respectively show the TerraSAR-X image time-series (all orbits combined) for the 2015-2016, 2016-2017, and 2017-2018 ice seasons. They are available online at https://doi.pangaea.de/10.1594/PANGAEA.911042 (Dufour-Beauséjour et al. 2019).

Author contributions: SDB participated in study design, data acquisition, analysis, and interpretation, and wrote the article. AW participated in study design, data analysis and interpretation, and wrote the article. YG participated in study design and data interpretation, and revised the article. MB participated in study design and revised the article. JP and VG participated in study design and data acquisition. JT and A. Roth participated in data acquisition. A. Rouleau participated in study design.

Competing interests: The authors declare that they have no conflict of interest.

Acknowledgements: The authors would like to thank the Inuit guides from Salluit who participated in data acquisition in Deception Bay (in alphabetical order): Chris Alaku, Johnny Ashevak, Michael Camera, Putulik Cameron, Charlie Ikey, Luuku Isaac, Markusi Jaaka, Adamie Raly Kadjulik, Joannasie Kakayuk, Jani Kenuajuak, Pierre Lebreux, Casey Mark, Denis Napartuk, Eyetsiaq Papigatuk, and Kululak Tayara. Thanks also to INRS students who also participated in data acquisition: Pierre-Olivier Carreau, Étienne Lauzier-Hudon. Thanks to Jasmin Gill-Fortin (INRS) for his help with the time-lapse photography data. We further thank Valérie Plante Lévesque (INRS), Charles Gignac (INRS), Randy Scharien (University of Victoria), Torsten Geldsetzer (Natural Resources Canada), and Derek Mueller (Carleton University) for their advice and suggestions on this manuscript, and Guillaume Légaré (INRS) for his advice on time-series analysis. Thanks to the German Space Agency (DLR) for providing the TerraSAR-X images, and for data processing with the MultiSAR-System. The authors acknowledge the use of TerraSAR-X (©DLR 2017-18). This study was done within the Ice Monitoring project, a research collaboration between the Kativik Regional Government (KRG), Raglan Mine, a Glencore company, Institut national de la recherche scientifique (INRS) and the Northern Villages of Salluit and Kangiqsujuaq.

Financial support: This INRS research was supported by Polar Knowledge Canada (Safe Passage, project number PKC-NST-1617-0003), Raglan Mine (a Glencore company), the Kativik Regional Government, the NSERC Discovery Grant -and the Northern Research Supplements Program (attributed to Pr. Monique Bernier), the Ministère des Transports du Québec, and the Northern Scientific Training Program (attributed to Sophie Dufour-Beauséjour). Ph.D. scholarships were provided to the first author by NSERC (Alexander Graham Bell Canada Graduate Scholarship – Doctoral) and the W. Garfield Weston Foundation (The W. Garfield Weston Awards for Northern Research).

References

Arslan, A. N., Tanis, C. M., Metsämäki, S., Aurela, M., Böttcher, K., Linkosalmi, M. and Peltoniemi, M.: Automated Webcam Monitoring of Fractional Snow Cover in Northern Boreal Conditions, Geosciences, 7(3), 55, https://doi.org/10.3390/geosciences7030055, 2017.

Barber, D. G. and Nghiem, S. V.: The role of snow on the thermal dependence of microwave backscatter over sea ice, J. Geophys. Res.-Oceans, 104(C11), 25789–25803, https://doi.org/10.1029/1999JC900181, 1999.

Barber, D. G., Papakyriakou, T. N., Ledrew, E. F. and Shokr, M. E.: An examination of the relation between the spring period evolution of the scattering coefficient (σ) and radiative fluxes over Jandfast sea-ice, Int. J. Remote Sens., 16(17), 3343–3363, https://doi.org/10.1080/01431169508954634, 1995.

Bernier, M., Poulin, J., Gilbert, V. and Rouleau, A.: Ice Monitoring: Hourly pictures of landfast sea ice from Deception Bay (Nunavik, Canada), Canadian Cryospheric Information Network (CCIN), 2017.

Bertram, A., Wendleder, A., Schmitt, A. and Huber, M.: Long-Term Monitoring of Water Dynamics in the Sahel Region using the Multi-SAR-System, in: The International Archives of the Photogrammetry, Remote Sensing and Spatial Information Sciences, XXIII ISPRS Congress, Commission VIII, Prague, Czech Republic, 12–19 July 2016, 8, 2016.

Bongio, M., Arslan, A. N., Tanis, C. M., and De Michele, C.: Snow Depth Estimation by Time-Lapse Photography: Finnish and Italian Case Studies, Preprint. Snow/Remote Sensing. https://doi.org/10.5194/tc-2019-193, 2019.

Cassotto, R., Fahnestock, M., Amundson, J. M., Truffer, M. and Joughin, I.: Seasonal and interannual variations in ice melange and its impact on terminus stability, Jakobshavn Isbræ, Greenland, J. Glaciol., 61(225), 76–88, https://doi.org/10.3189/2015JoG13J235, 2015.

Chauché, N., Hubbard, A., Gascard, J.-C., Box, J. E., Bates, R., Koppes, M., Sole, A., Christoffersen, P. and Patton, H.: Ice–ocean interaction and calving front morphology at two west Greenland tidewater outlet glaciers, The Cryosphere, 8(4), 1457–1468, https://doi.org/10.5194/tc-8-1457-2014, 2014.

Christiansen, H. H.: Snow-cover depth, distribution and duration data from northeast Greenland obtained by continuous automatic digital photography, Ann. Glaciol., 32, 102–108, https://doi.org/10.3189/172756401781819355, 2001.

Cuerrier, A., Brunet, N. D., Gérin-Lajoie, J., Downing, A. and Lévesque, E.: The Study of Inuit Knowledge of Climate Change in Nunavik, Quebec: A Mixed Methods Approach, Hum. Ecol., 43(3), 379–394, https://doi.org/10.1007/s10745-015-9750-4, 2015.

Dufour-Beauséjour, S.: tiffstats, Zenodo, http://doi.org/10.5281/zenodo.3352367, 2019.

Dufour-Beauséjour, S.; Wendleder, A.; Gauthier, Y.; Bernier, M.; Poulin, J.; Gilbert, V.; Tuniq, J.; Rouleau, A.: Freeze-up and break-up observations in Nunavik's Deception Bay from TerraSAR-X and time-lapse photography, PANGAEA, https://doi.pangaea.de/10.1594/PANGAEA.904960, 2019.

Dumont, M., Sirguey, P., Arnaud, Y., and Six, D.: Monitoring Spatial and Temporal Variations of Surface Albedo on Saint Sorlin Glacier (French Alps) Using Terrestrial Photography, The Cryosphere 5 (3): 759–71, https://doi.org/10.5194/tc-5-759-2011, 2011.

Eineder, M., Fritz, T., Mittermayer, J., Roth, A., Boerner, E. and Breit, H.: TerraSAR-X Ground Segment, Basic Product Specification Document, CAF - Cluster Applied Remote Sensing., Germany, 2008.

Eriksson, L. E. B., Pemberton, P., Lindh, H. and Karlson, B.: Evaluation of new spaceborne SAR sensors for sea-ice monitoring in the Baltic Sea, Can. J. Remote Sens., 36(1), S56–S73, https://doi.org/10.5589/m10-020, 2010.

Farinotti, D., Magnusson, J., Huss, M. and Bauder, A.: Snow accumulation distribution inferred from time-lapse photography and simple modelling, Hydrol. Process., 24(15), 2087–2097, https://doi.org/10.1002/hyp.7629, 2010.

Fequet, D., Hache, L., McCourt, S., Langlois, D., Dicaire, C., Premont, B., Jolicoeur, A. and Minano, A.: Sea Ice Climatic Atlas: Northern Canadian Waters 1981–2010, En56-173-2010–1, Canadian Ice Service, Environnement Canada, Ottawa, Ont.., 2011.

Fors, A. S., Brekke, C., Doulgeris, A. P., Eltoft, T., Renner, A. H. H. and Gerland, S.: Late-summer sea ice segmentation with multi-polarisation SAR features in C and X band, The Cryosphere, 10(1), 401–415, https://doi.org/10.5194/tc-10-401-2016, 2016.

Gauthier, Y., Dufour-Beauséjour, S., Poulin, J., and Bernier, M. 2018. *Ice Monitoring in Deception Bay : Progress report 2016-2018*. Québec: INRS, Centre Eau Terre Environnement. http://espace.inrs.ca/7538/.

GENIVAR: Environmental and Social Impact Assessment of the Deception Bay Wharf and Sediment Management, Report from GENIVAR for Canadian Royalties Inc., Montreal, Que., 2012.

Gill, J. P. S., Yackel, J. J., Geldsetzer, T. and Fuller, M. C.: Sensitivity of C-band synthetic aperture radar polarimetric parameters to snow thickness over landfast smooth first-year sea ice, Remote Sens. Environ., 166, 34–49, https://doi.org/10.1016/j.rse.2015.06.005, 2015.

Gogineni, S. P., Moore, R. K., Grenfell, T. C., Barber, D., Digby, S. and Drinkwater, M.: The effects of freeze-up and melt processes on microwave signatures, in Microwave remote sensing of sea ice, Geophys. Monogr. vol. 68, edited by F. D. Carsey, pp. 329–341., Washington, DC, 1992.

Herdes, E., Copland, L., Danielson, B. and Sharp, M.: Relationships between iceberg plumes and sea-ice conditions on northeast Devon Ice Cap, Nunavut, Canada, Ann. Glaciol., 53(60), 1–9, https://doi.org/10.3189/2012AoG60A163, 2012.

Ide, R. and Oguma, H.: A cost-effective monitoring method using digital time-lapse cameras for detecting temporal and spatial variations of snowmelt and vegetation phenology in alpine ecosystems, Ecol. Inform., 16, 25–34, https://doi.org/10.1016/j.ecoinf.2013.04.003, 2013.

Isleifson, D., Galley, R. J., Barber, D. G., Landy, J. C., Komarov, A. S. and Shafai, L.: A Study on the C-Band Polarimetric Scattering and Physical Characteristics of Frost Flowers on Experimental Sea Ice, IEEE Transactions on Geoscience and Remote Sensing, 52(3), 1787–1798, https://doi.org/10.1109/TGRS.2013.2255060, 2014.

Johansson, A. M., King, J. A., Doulgeris, A. P., Gerland, S., Singha, S., Spreen, G. and Busche, T.: Combined observations of Arctic sea ice with near-coincident colocated X-band, C-band, and L-band SAR satellite remote sensing and helicopter-borne measurements, J. Geophys. Res.-Oceans, 122(1), 669–691, https://doi.org/10.1002/2016JC012273, 2017.

Johansson, A. M., Brekke, C., Spreen, G. and King, J. A.: X-, C-, and L-band SAR signatures of newly formed sea ice in Arctic leads during winter and spring, Remote Sens. Environ., 204, 162–180, https://doi.org/10.1016/j.rse.2017.10.032, 2018.

Kępski, D., Luks, B., Migała, K., Wawrzyniak, T., Westermann, S. and Wojtuń, B.: Terrestrial remote sensing of snowmelt in a diverse High-Arctic tundra environment using time-lapse imagery, Remote Sens., 9(7), 733, https://doi.org/10.3390/rs9070733, 2017.

Kim, Y.-S., Onstott, R. and Moore, R.: Effect of a snow cover on microwave backscatter from sea ice, IEEE J. Oceanic Eng., 9(5), 383–388, https://doi.org/10.1109/JOE.1984.1145649, 1984.

Laidler, G. J., and Ikummaq, T.: Human Geographies of Sea Ice: Freeze/Thaw Processes around Igloolik, Nunavut, Canada. Polar Record 44 (02), https://doi.org/10.1017/S0032247407007152, 2008.

Liu, J., Chen, R., Song, Y., Yang, Y., Qing, W., Han, C. and Liu, Z.: Observations of precipitation type using a time-lapse camera in a mountainous region and calculation of the rain/snow proportion based on the critical air temperature, Environ. Earth Sci., 73(4), 1545–1554, https://doi.org/10.1007/s12665-014-3506-0, 2015.

Mailhot, A. and Chaumont, D.: Élaboration du portrait bioclimatique futur du Nunavik - Tome II. Rapport présenté au Ministère de la forêt, de la faune et des parcs., Ouranos, Montreal, Que., 2017.

Matsuoka, T., Uratsuka, S., Satake, M., Kobayashi, T., Nadai, A., Umehara, T., Maeno, H., Wakabayashi, H., Nakamura, K. and Nishio, F.: CRL/NASDA airborne SAR (Pi-SAR) observations of sea ice in the Sea of Okhotsk, Ann. Glaciol., 33, 115–119, https://doi.org/10.3189/172756401781818734, 2001.

Mussells, O., Dawson, J., and Howell, S.: Navigating Pressured Ice: Risks and Hazards for Winter Resource-Based Shipping in the Canadian Arctic, Ocean & Coastal Management 137 (March): 57–67, https://doi.org/10.1016/j.ocecoaman.2016.12.010, 2017.

Nakamura, K., Wakabayashi, H., Naoki, K., Nishio, F., Moriyama, T. and Uratsuka, S.: Observation of sea-ice thickness in the sea of Okhotsk by using dual-frequency and fully polarimetric airborne SAR (pi-SAR) data, IEEE T. Geosci. Remote, 43(11), 2460–2469, https://doi.org/10.1109/TGRS.2005.853928, 2005.

Nandan, V., Geldsetzer, T., Islam, T., Yackel, John. J., Gill, J. P. S., Fuller, Mark. C., Gunn, G. and Duguay, C.: Ku-, X- and C-band measured and modeled microwave backscatter from a highly saline snow cover on first-year sea ice, Remote Sens. Environ., 187, 62–75, https://doi.org/10.1016/j.rse.2016.10.004, 2016.

Nghiem, S. V., S. Martin, D. K. Perovich, R. Kwok, R. Drucker, and A. J. Gow. 1997. "A Laboratory Study of the Effect of Frost Flowers on C Band Radar Backscatter from Sea Ice." *Journal of Geophysical Research: Oceans*102 (C2): 3357–70. https://doi.org/10.1029/96JC03208.

Nickels, S., Furgal, C., Buell, M. and Moquin, H.: Unikkaaqatigiit – Putting the Human Face on Climate Change: Perspectives from Inuit in Canada, Pre-release English only version., Inuit Tapiriit Kanatami, Nasivvik Centre for Inuit Health and Changing Environments at Université Laval and the Ajunnginiq Centre at the National Aboriginal Health Organization, Ottawa, Ont., 2005.

Onstott, R. G.: SAR and Scatterometer Signatures of Sea Ice, in: Microwave Remote Sensing of Sea Ice, American Geophysical Union, Washington, D.C., United States, 73-104, 1992.

Paul, S., Willmes, S., Hoppmann, M., Hunkeler, P. A., Wesche, C., Nicolaus, M., Heinemann, G. and Timmermann, R.: The impact of early-summer snow properties on Antarctic landfast sea-ice X-band backscatter, Ann. Glaciol., 56(69), 263–273, https://doi.org/10.3189/2015AoG69A715, 2015.

Peltoniemi, M., Aurela, M., Bottcher, K., Kolari, P., Loehr, J., Karhu, J., Linkosalmi, M., Tanis, C. M., Tuovinen, J.-P. and Arslan, A. N.: Webcam network and image database for studies of phenological changes of vegetation and snow cover in Finland, image time series from 2014 to 2016, Earth Syst. Sci. Data, 10(1), 173–184, https://doi.org/10.5194/essd-10-173-2018, 2018.

Petit, J.-G., Viger, Y. B., Aatami, P. and Iserhoff, A.: Les Inuit et les Cris du Nord du Québec: Territoire, gouvernance, société et culture, PUQ, Quebec, Que., 2011.

Revuelto, J., Jonas, T. and López-Moreno, J.-I.: Backward snow depth reconstruction at high spatial resolution based on time-lapse photography, Hydrol. Process., 30(17), 2976–2990, https://doi.org/10.1002/hyp.10823, 2016.

Scharien, R. K., Yackel, J. J., Barber, D. G., Asplin, M., Gupta, M. and Isleifson, D.: Geophysical controls on C band polarimetric backscatter from melt pond covered Arctic first-year sea ice: Assessment using high-resolution scatterometry, J. Geophys. Res.-Oceans, 117(C00G18), https://doi.org/10.1029/2011JC007353, 2012.

Schmitt, A., Wendleder, A. and Hinz, S.: The Kennaugh element framework for multi-scale, multi-polarized, multi-temporal and multi-frequency SAR image preparation, ISPRS J. Photogramm., 102, 122–139, https://doi.org/10.1016/j.isprsjprs.2015.01.007, 2015.

Smith Jr, K. L., Baldwin, R. J., Glatts, R. C., Chereskin, T. K., Ruhl, H. and Lagun, V.: Weather, ice, and snow conditions at Deception Island, Antarctica: long time-series photographic monitoring, Deep-Sea Res. Pt. II, 50(10–11), 1649–1664, https://doi.org/10.1016/S0967-0645(03)00084-5, 2003.

Sobiech, J., Boike, J. and Dierking, W.: Observation of melt onset in an arctic tundra landscape using high resolution TerraSAR-X and RADARSAT-2 data, in 2012 IEEE International Geoscience and Remote Sensing Symposium, 3552–3555, 2012.

Stettner, S., Lantuit, H., Heim, B., Eppler, J., Roth, A., Bartsch, A. and Rabus, B.: TerraSAR-X Time Series Fill a Gap in Spaceborne Snowmelt Monitoring of Small Arctic Catchments—A Case Study on Qikiqtaruk (Herschel Island), Canada, Remote Sens., 10(7), 1155, https://doi.org/10.3390/rs10071155, 2018.

Tuniq J, Usuituayuk T, Saviadjuk P, Papigatuk Lebreux I, Delisle Alaku A and Cameron M. 2017. Observations of Arctic Change from Salluit, Nunavik. Presented at Arctic Change 2017, Quebec, Canada.

Ulaby, F. T., R. K. Moore, and A. K. Fung. 1986. *Microwave Remote Sensing: Active and Passive.* Vol. Volume 3-From theory to applications. United States: Addison-Wesley Publishing Company. https://ntrs.nasa.gov/search.jsp?R=19860041708.

Vogel, S., Eckerstorfer, M. and Christiansen, H. H.: Cornice dynamics and meteorological control at Gruvefjellet, Central Svalbard, The Cryosphere, 6(1), 157–171, https://doi.org/10.5194/tc-6-157-2012, 2012.

WMO: Sea-Ice Nomenclature, No. 259, World Meteorological Organization, Switzerland, 2014.

Wobus, C., Anderson, R., Overeem, I., Matell, N., Clow, G. and Urban, F.: Thermal Erosion of a Permafrost Coastline: Improving Process-Based Models Using Time-Lapse Photography, Arct. Antarct. Alp. Res., 43(3), 474–484, https://doi.org/10.1657/1938-4246-43.3.474, 2011.

Yackel, J. J., Barber, D. G., Papakyriakou, T. N. and Breneman, C.: First-year sea ice spring melt transitions in the Canadian Arctic Archipelago from time-series synthetic aperture radar data, 1992–2002, Hydrol. Process., 21(2), 253–265, https://doi.org/10.1002/hyp.6240, 2007.

Zhang, E., Liu, L. and Huang, L.: Automatically delineating the calving front of Jakobshavn Isbræ from multitemporal TerraSAR-X images: a deep learning approach, The Cryosphere, 13(6), 1729–1741, https://doi.org/10.5194/tc-13-1729-2019, 2019.